



EUROPEAN  
COMMISSION

Community research



GOBIERNO  
DE ESPAÑA

MINISTERIO  
DE ECONOMÍA  
Y COMPETITIVIDAD

**Ciemat**  
Centro de Investigaciones  
Energéticas, Medioambientales  
y Tecnológicas



Long-term  
Performance of  
Engineered  
Barrier  
Systems

## Long-term Performance of Engineered Barrier Systems PEBS

# EB experiment Laboratory infiltration tests report

**(DELIVERABLE-Nº: D2.1-5)**

**Contract (grant agreement) number: FP7 249681**

CIEMAT Technical Report CIEMAT/DMA/2G210/03/2012

Author(s):

M.V. Villar

Reporting period:

Date of issue of this report: October 31<sup>st</sup> 2012

Start date of project: 01/03/10

Duration : 48 Months

**Project co-funded by the European Commission under the Seventh Euratom Framework Programme for Nuclear Research & Training Activities (2007-2011)**

### Dissemination Level

<b>PU</b>	Public	<b>PU</b>
<b>RE</b>	Restricted to a group specified by the partners of the [acronym] project	
<b>CO</b>	Confidential, only for partners of the [acronym] project	

PEBS





# Contents

- Contents..... I**
- 1 Introduction..... 1**
- 2 Material..... 2**
- 3 Methodology..... 4**
  - 3.1 Experimental setups ..... 4
  - 3.2 Post-mortem analysis..... 6
- 4 Results..... 8**
  - 4.1 TEST INF\_PELL1..... 8
  - 4.2 Test MGR13 ..... 13
  - 4.3 Test MGR14 ..... 19
- 5 Summary and discussion..... 24**
- Conclusions..... 31**
- Acknowledgements..... 33**
- References ..... 33**



# 1 Introduction

The EB experiment (ENRESA 2005), run by ENRESA at the Mont Terri Underground Research Laboratory in Switzerland, started in October 2000 with the aim of demonstrating that automated production of a Granular Bentonite Material (GBM) and its emplacement in the upper part of a clay barrier were feasible. The EB niche is 15 m long and has a geometry of a horseshoe section, 2.55 m high and 3 m wide (Figure 1).

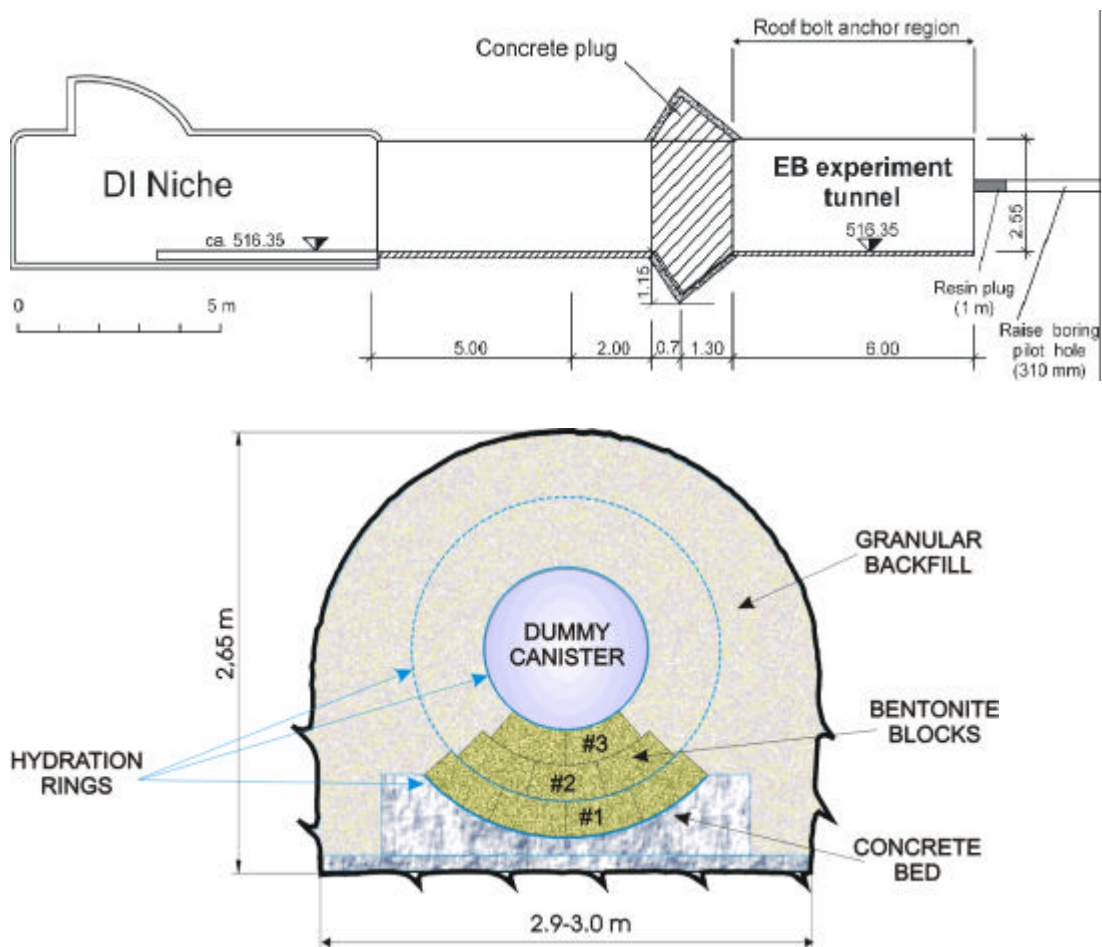


**Figure 1: EB niche at Mont Terri URL, longitudinal and cross sections**

In the EB test section an average dry density of  $1.36 \text{ g/cm}^3$  of the emplaced GBM was obtained, although some segregation during the emplacement and density inhomogeneities could have occurred. According to the laboratory characterization of the GBM (ENRESA 2005), for this dry density value it was estimated that the hydraulic conductivity was lower than  $5 \cdot 10^{-12} \text{ m/s}$  and the swelling pressure about 1.3 MPa. The artificial hydration of the buffer material started on May 2002 and was carried out with Pearson water coming from a deposit. The Pearson water is a sodium-rich solution and has a composition similar to the Opalinus Clay formation pore water. It has a density of  $1.020 \text{ g/cm}^3$  (Pearson 1998) and the chemical composition is indicated in Table I.

**Table I: Chemical composition of Pearson water (mg/L)**

Cl <sup>-</sup>	SO <sub>4</sub> <sup>2-</sup>	HCO <sub>3</sub> <sup>-</sup>	Mg <sup>2+</sup>	Ca <sup>2+</sup>	Na <sup>+</sup>	K <sup>+</sup>	Sr <sup>+</sup>	pH
10635.90	1354.41	25.75	413.19	1034.06	5550.01	62.95	44.69	7.6

The performance of tests at different scales, in both the laboratory and the field, is also very useful to observe the thermo-hydro-mechanical processes taking place in the engineered barriers and the geological medium. They also provide the information required for the verification and validation of mathematical models of the coupled processes and their numerical implementation. The laboratory tests in cells are particularly helpful to identify and quantify processes in a shorter period of time and with less uncertainty regarding the boundary conditions than the *in situ* tests. Since the hydration of a shaft or tunnel seal due to the inflow of host rock water is performed under the confinement provided by the excavation walls, swelling pressure tests are very appropriate to examine the behaviour relevant to seal hydration (Gens *et al.* 2011).

Thus, to complement the information provided by the EB *in situ* test, CIEMAT undertook the performance of tests in cells simulating the saturation of the pellets mixture used in the *in situ* test. The aim of these tests was:

- To provide support for the modelling of the EB *in situ* test
- To check the long-term hydro-mechanical behaviour of a pellets barrier
- To compare the HM behaviour of pellets and compacted bentonite

The description of the experimental setups and materials used as well as the results obtained in these tests are given in this report.

## 2 Material

The GBM used in the EB experiment was prepared from FEBEX bentonite dried and milled in a three-step process to produce a fine grade powder with a water content of 3.3%. Later, a commercial plant with an in-line highly automated briquetting process produced coarse (>7 mm) and fine (0.4-2 mm) grained materials with dry densities of 2.11 and 2.13 g/cm<sup>3</sup>, respectively. These two grain size fractions were subsequently combined after several trials to produce a material with a granulometric Simonis curve, which was used for the *in situ* emplacement (ENRESA 2005).

The material used in the laboratory tests is the same as in the *in situ* test and was sent to CIEMAT through UPC in October 2006 (9 kg). The material had an initial water content of 4.7%. It was checked that the granulometric curve of the bentonite pellets received at CIEMAT coincide with the granulometric curve of the material used in UPC (Hoffmann 2005). These curves could be fit to a Fuller shape curve (Figure 2). To prepare the samples in the laboratory it was decided to follow a Fuller fitting modified to have a maximum diameter of 12.7 mm and a minimum diameter of 0.425 mm, in order to reduce segregation. Thus, the different grain sizes were kept separated and mixed in the right proportion before every test.

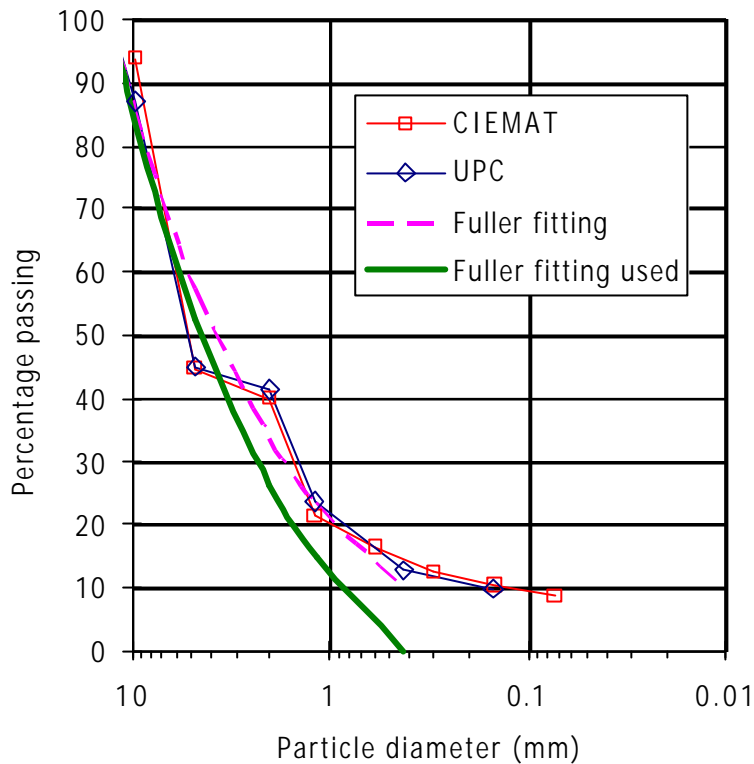


**Figure 2: Granulometric curve of the material used *in situ* as determined at CIEMAT and UPC laboratories, Fuller fitting for this curves, and Fuller fitting used in the laboratory tests**

The physico-chemical properties of the FEBEX bentonite, as well as its most relevant thermo-hydro-mechanical and geochemical characteristics obtained during the projects FEBEX I and II were summarised in the final report of the project (ENRESA 2006). The FEBEX bentonite was extracted from the Cortijo de Archidona deposit (Almería, Spain). The processing at the factory consisted of disaggregation and gently grinding, drying at 60°C and sieving by 5 mm, and this was the material used for the laboratory characterisation.

The montmorillonite content of the FEBEX bentonite is above 90 wt.%. The smectitic phases are actually made up of a smectite-illite mixed layer, with 10-15 wt.% of illite layers. Besides, the bentonite contains variable quantities of quartz, plagioclase, K-felspar, calcite, and cristobalite-trydimite. The liquid limit of the bentonite is 102±4%, the plastic limit 53±3%, the specific gravity 2.70±0.04, and 67±3 percent of particles are smaller than 2 µm. The hygroscopic water content is 13.7±1.3 percent. The total specific surface area obtained using the Keeling hygroscopicity method is 725 m<sup>2</sup>/g. The cation exchange capacity is 102±4 meq/100g, the main exchangeable cations being calcium, magnesium and sodium. The predominant soluble ions are chloride, sulphate, bicarbonate and sodium.

The saturated hydraulic conductivity to deionised water ( $k_w$ , m/s) of samples of untreated FEBEX bentonite compacted at different dry densities is exponentially related to dry density ( $\rho_d$ , g/cm<sup>3</sup>). A distinction may be made between two different empirical fittings depending on the density interval:

for dry densities of less than 1.47 g/cm<sup>3</sup>:

$$\log k_w = -6.00 \rho_d - 4.09 \quad [1]$$

for dry densities in excess of 1.47 g/cm<sup>3</sup>:

$$\log k_w = -2.96 \rho_d - 8.57 \quad [2]$$

The determinations were done at room temperature. The variation in the experimental values with respect to these fittings is smaller for low densities than it is for higher values, with an average –in absolute values– of 30 percent.

The swelling pressure ( $P_s$ , MPa) of FEBEX samples compacted with their hygroscopic water content and flooded with deionised water up to saturation at room temperature and constant volume conditions can be related to dry density ( $\rho_d$ , g/cm<sup>3</sup>) through the following equation:

$$\ln P_s = 6.77 \rho_d - 9.07 \quad [3]$$

In this case, the difference between experimental values and this fitting is, on average, 25 percent.

Although this characterisation was performed in granular material with a grain size <5 mm, it was proved that the saturated hydro-mechanical properties of pellets mixtures are similar to those of granulates (Imbert & Villar 2006). Hoffmann (2005) performed permeability tests in a FEBEX pellets mixture (with the granulometric curve shown in Figure 2) and found the following experimental relation for dry densities between 1.0 and 1.6 g/cm<sup>3</sup>, which gives higher permeability values than Equation 1:

$$\ln k_w = -9.73 \rho_d - 13.79 \quad [4]$$

## 3 Methodology

### 3.1 EXPERIMENTAL SETUPS

The saturation tests were performed in two kinds of cylindrical stainless steel cells in which the pellets were poured and compacted. One of them was a very simple rigid cell and the other one a large-scale oedometer.

#### 3.1.1 Rigid cell

This cylindrical hermetic cell had an internal height of 100 mm and diameter of 70 mm and was made of stainless steel (Figure 3). The upper lid of the cell had a central perforation onto which a screw fitting connected to a tube was threaded. The imperviousness of the cell was guaranteed by using sealing adhesive between the cell body and the covers and in the upper hole.

The pellets mixture prepared according to the curve shown in Figure 2 was directly compacted inside the cell. To ease a homogeneous distribution of water over the sample surface, a filter paper and a 8-mm high porous stone were placed on top of the bentonite; consequently, the initial height of the sample was 9.2 cm.

Saturation took place with deionised water from a water deposit initially located 1.4 m over the cell. The cell with the sample in it was placed on a balance to check the water intake during saturation. In addition, an automatic volume change apparatus placed between the water deposit and the cell measured the water intake (Figure 4). After 72 h hydration the injection pressure was increased to 200 kPa. Both the balance and the volume change apparatus were connected to a data acquisition system that recorded both parameters online during the whole duration of the test. The test was performed at laboratory temperature.

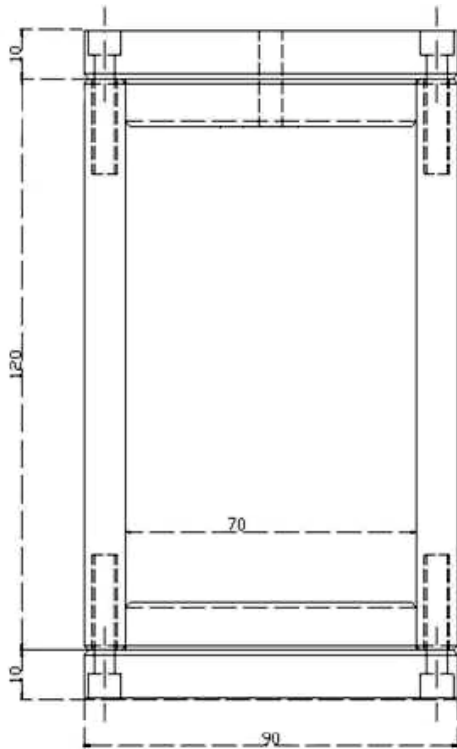


Figure 3: Schematic design of the rigid cell

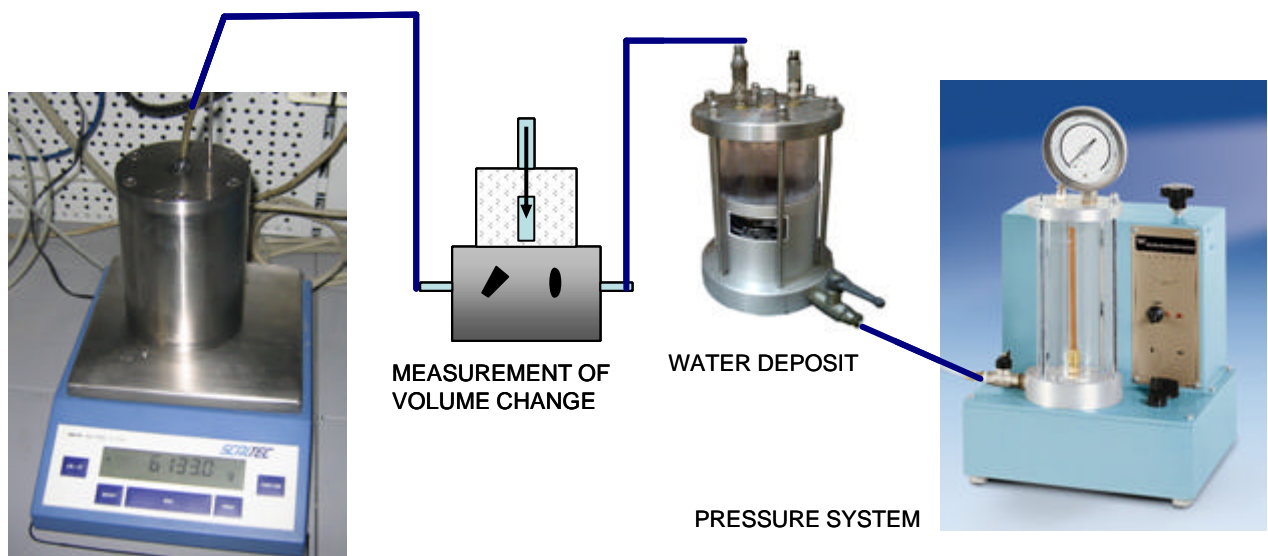


Figure 4: Setup for the performance of the hydration test INF\_PELL1

### 3.1.2 Large oedometric cell

The large-scale oedometer was specially designed to work with pellets/powder mixtures and it consisted of a cylindrical body with base and an upper piston that may move in the cylinder (Imbert & Villar 2006). The body had an inner diameter of 10.0 cm and the length of the sample inside may be 10 or 5 cm. The top and bottom of the sample were in contact with ceramic porous discs connected to outlets. The cell was placed in a rigid frame that guaranteed the constant volume of the sample by hindering the displacement of the piston. Nevertheless, an external LVDT measured the potential axial displacements, whereas a load cell in the upper part of the frame measured the force developed by the specimen. This was a 5-t cell for test MGR13

and a 2-t cell for test MGR14. The water intake, which took place through the bottom surface, was measured by an automatic volume change apparatus.

Once in the oedometer frame, the samples were saturated by the bottom face, while the top outlet remained initially open to atmosphere and the pressure exerted by the clay, the sample deformation and the water intake were measured and automatically recorded. The water used was deionised and the tests were performed at laboratory temperature.

In test MGR13, after full saturation of the sample, the hydraulic conductivity was measured. For that, the pressure at the bottom of the sample was increased to 1200 kPa, and a lower pressure (600 kPa) was applied to the top of the sample by means of an oil/water pressure system. Both the water inlet and outlet were measured by means of automatic volume change apparatuses placed between the pressure systems and the sample cell.

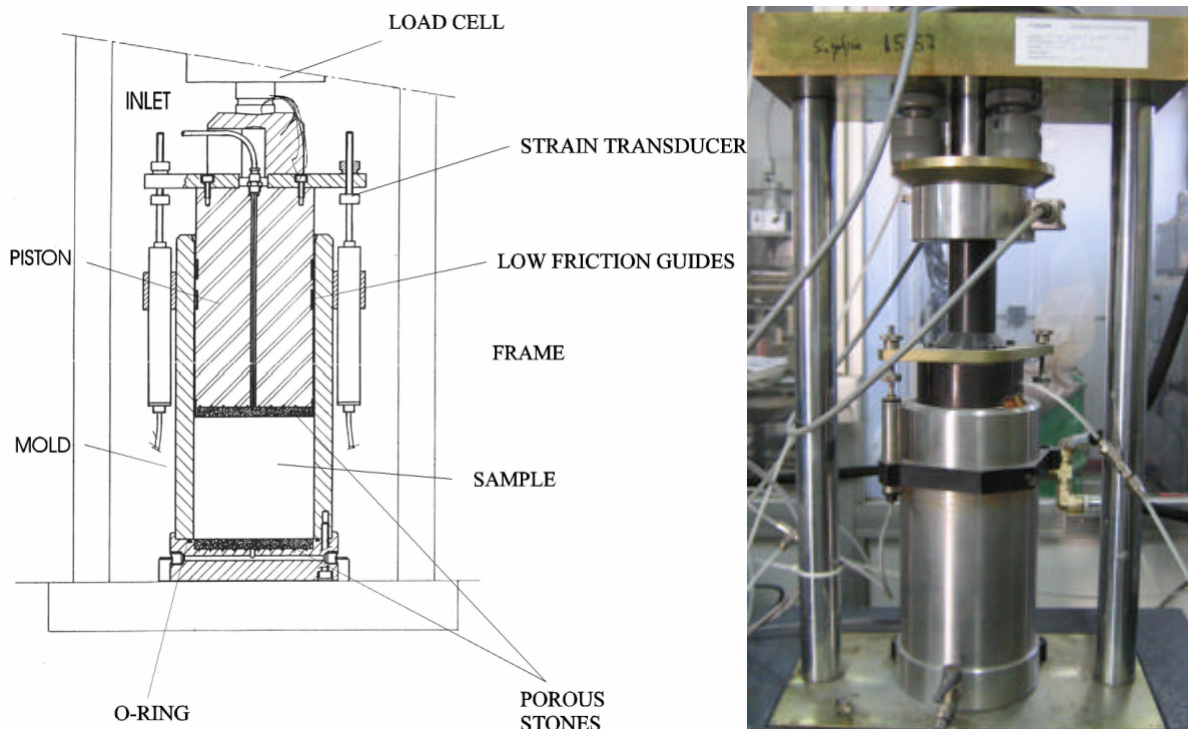


**Figure 5: Schematic design and appearance of the large oedometer cell used for tests MGR13 and MGR14**

### 3.2 POST-MORTEM ANALYSIS

After dismantling, the cylindrical blocks were subsampled to determine the water content and dry density at different levels.

The gravimetric water content ( $w$ ) is defined as the ratio between the weight of water and the weight of dry solid expressed as a percentage. The weight of water was determined as the difference between the weight of the sample and its weight after oven drying at 110°C for 48 h (weight of solid). Dry density ( $\rho_d$ ) is defined as the ratio between the weight of the dry sample and the volume occupied by it prior to drying. The volume of the specimens was determined by immersing them in a recipient containing mercury and by weighing the mercury displaced, as established in UNE Standard 7045 "Determination of soil porosity".

Mercury intrusion porosimetry tests, determination of the specific surface area and measurement of the basal spacing of the smectite were done in all the subsamples according to the procedures described below.

### 3.2.1 Pore size distribution

The pore size distribution of the samples was determined by mercury intrusion porosimetry (MIP). This technique allows the determination of pore size distribution by injecting mercury into the sample at different pressures while controlling the volume intruded. The pressure applied may be related to the minimum pore diameter intruded, taking into account the characteristics of the fluid. The ratio of the volume of mercury intruded (pore volume) to applied pressure (which conditions the minimum pore diameter) allows distribution curves to be obtained establishing the percentage of pores of a size included within a given range.

Samples of sizes lower than 3 cm<sup>3</sup> were cut and put in the ice condenser of a Telstar LioQuest equipment at -50°C for 3 h. Afterwards they were lyophilised for 19 h at a temperature of -50°C under a vacuum of 0.2 mbar, so that to eliminate the water in the pores by sublimation. Before the MIP tests the samples were heated to 35°C in 2 h. The porosimeter used was a Micromeritics AutoPore Series IV 9500, which applied a maximum injection pressure of 31900 psi, allowing the exploration of pore diameters between 0.007 and 500 µm. Prior to mercury injection the sample was outgassed by applying a vacuum of 50 µmHg. Afterwards the mercury injection pressure was increased from 0.36 to 31900 psi in 110 steps. To determine the extrusion branch of the curve, the pressure was released in 57 steps down to a pressure of 4.44 psi. A contact angle of mercury of 139° both on advancing and of receding on the clay surface was considered.

The mercury does not intrude the microporosity (pores of a size of less than 0.002 µm, according to the classification of Sing *et al.* 1985), but only the macroporosity and part of the mesopores. The percentage of pores not intruded by mercury includes not only those whose sizes are below 0.007 µm or above 500 µm, but also those whose entrance pore size is below that value or those isolated, even if the pores themselves are larger. The percentage of pores not intruded can be computed by comparing the actual void ratio of the samples (computed from their dry density and solid specific gravity measured by pycnometers) and the apparent void ratio calculated from mercury intrusion. Then, assuming that the percentage of pores not intruded in a clay corresponds entirely to the micropore size, the percentage of micropores can be estimated. Alternatively, Delage & Lefebvre (1984) suggested that microporosity could be estimated from the trapped volumes after mercury extrusion.

### 3.2.2 Nitrogen adsorption isotherms

The nitrogen adsorption isotherms were determined in some of the samples previously lyophilised as described above, what allowed the measurement of the specific surface area and the micropore volume. The equipment used was a Micromeritics ASAP 2020.

Prior to the nitrogen adsorption, the samples were outgassed using a mixture of helium and nitrogen at 90°C, temperature reached at a rate of 3°C/min. The outgassing was performed at 5 mm Hg/s, until reaching a vacuum of 100 µm Hg, at which the sample was kept for 10 min. The heating phase at 90°C lasted 420 min. After this process the sample was considered free from moisture and impurities and the tests were performed at the boiling point of liquid nitrogen (77 K). Surface areas were calculated with the BET method, which is based on the determination of the quantity of gas adsorbed in a monolayer of molecules and the consideration that this quantity is proportional to the surface area of the material. A series of nine data points over the  $P/P_0$  range of 0.05 to 0.25 on the nitrogen adsorption isotherm were used. A molecular cross section area of 0.162 nm<sup>2</sup> was considered for the nitrogen molecule.

### 3.2.3 X-ray diffraction

X-ray profiles were registered in the samples to determine the smectite basal spacing. For that, the X-ray profiles of a sufficiently flat surface of the samples were registered at room temperature without any previous treatment. An anticatode of Cu ( $\text{CuK}\alpha$ ) radiation was used with a Philips model X'Pert-MPD diffractometer at 40 mA, 45 kV operating condition. X-ray diffraction (XRD) experimental profiles were obtained with a 0.1 mm entrance slit and a scanning rate of  $0.02^\circ 2\theta/\text{s}$ . Data were collected from  $0.2$  to  $30^\circ 2\theta$ . The position of the peaks was adjusted by using the quartz in the samples as an internal standard. A profile function was fitted to the observed intensities in order to obtain better peak parameters (peak position, net intensity and full width at half maximum (FWHM)) completely describing the measured scan. The pseudo-Voigt profile function, which is the weighted mean between a Lorentz and a Gaussian function, was used. It was also used to deconvolute overlapped peaks. The basal spacings thus determined are given in nm.

The gravimetric water content ( $w$ ) of the bentonite was determined by oven drying at  $110^\circ\text{C}$  during 48 hours in the specimens after X-ray diffraction. The comparison of this water content with that of an adjacent sample not submitted to X-ray diffraction allowed to assess the drying of the samples caused by the radiation process, which was generally judged not significant.

## 4 Results

### 4.1 TEST INF\_PELL1

This test was conducted in the rigid cell described in section 3.1.1. The pellets mixture prepared according to the curve shown in Figure 2 was directly compacted inside the cell at a nominal dry density of  $1.36 \text{ g/cm}^3$  with a nominal water content of 4.7% by applying a uniaxial pressure of 1.5 MPa. These values were checked at the end of the test and resulted to be actually  $1.35 \text{ g/cm}^3$  and 5.3%. The block had an initial diameter of 7.0 cm and a height of 9.2 cm.

#### 4.1.1 Online measurements

The test started in December 2006 and was dismantled in August 2011, it lasted 1703 days. During the first 3 days a 1.4-m water column was used to saturate the sample, and then the injection pressure was fixed to 200 kPa and kept so for the rest of the test. The evolution of water intake as measured by the volume change apparatus and by the balance, along with the temperature in the laboratory during the test, are shown in Figure 6. The measurements obtained with the two methods are quite coherent, except for the last 100 days, when the volume change recorded a decrease in water intake while there was no change in the cell weight.

Most of the water intake took place in the first 150 days and then continued in a softer way until approximately day 1200, when full saturation seemed to have taken place, since no noticeable further change in cell weight or water intake were recorded. According to the final online measurements, the final water content would be between 48.8% (volume change) and 49.7% (weight cell change). Nevertheless, it was checked at the end of the test that the actual final water intake had been much lower, as it is indicated in the Figure, and that the online measurement overestimated the water intake by a 29%. It is difficult to say which is the source of these faulty measurements, since in the last part of the test both measurements stabilised.

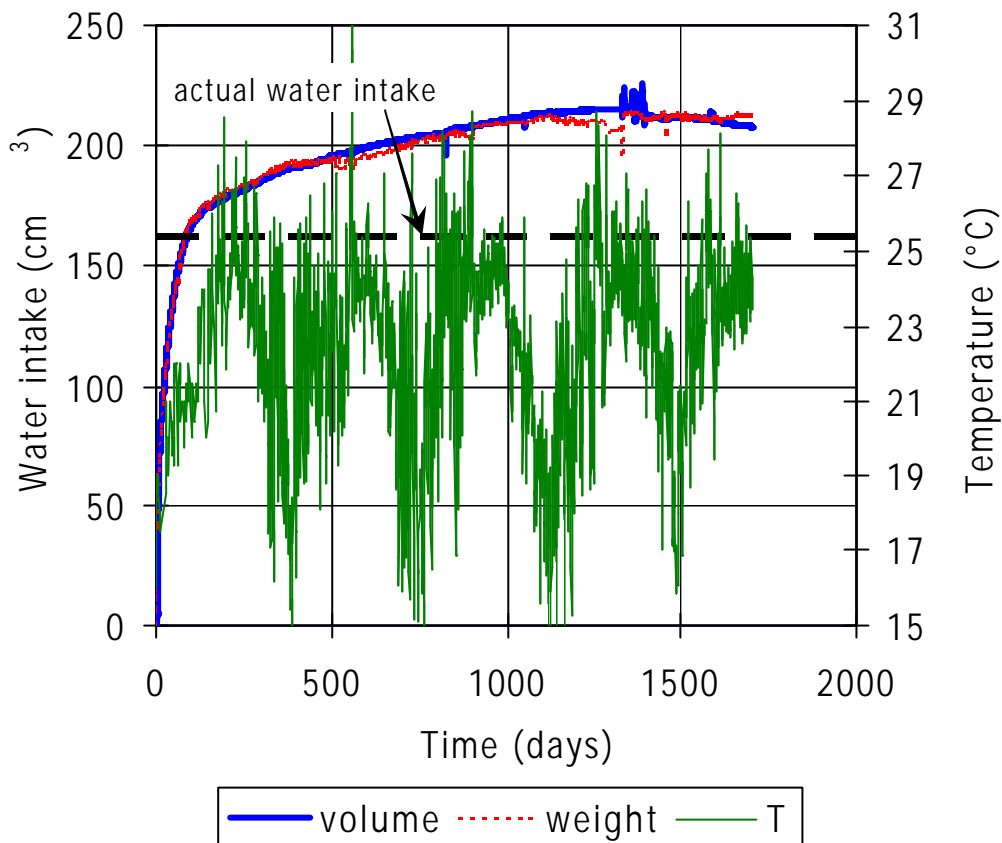


**Figure 6: Evolution of water intake and temperature during test INF\_PELL1**

#### 4.1.2 Post mortem analysis

After 1703 days operation (4.7 years) the cell was dismantled. The block was extracted, weighed and its dimensions measured. It was cut in five sections in which the different post mortem determinations were performed. The block displayed a perfectly saturated, homogeneous appearance and no pellets could be identified (Figure 7).



**Figure 7: Appearance of sample INF\_PELL1 after extraction**

From the final dimensions measurement the dry density of the block was  $1.33 \text{ g/cm}^3$  and its final water content 39.1%, this would correspond to a degree of saturation of 102%. Figure 8 shows the measurements performed in the five equal levels in which the block was subsampled. The average dry density measured in the subsamples was  $1.32 \text{ g/cm}^3$ , lower than that calculated from the dimensions due to the fact that cutting for subsampling usually implies a slight decrease in dry density. The sample closest to the hydration surface had the highest water content and lowest dry density.

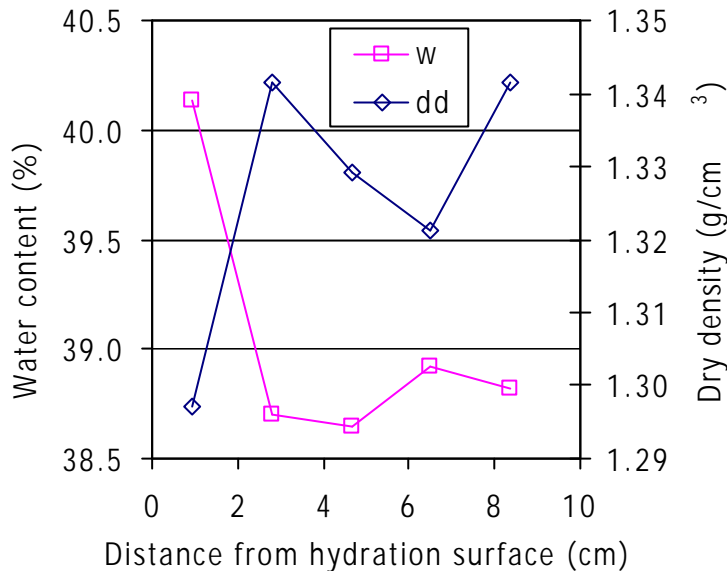


**Figure 8: Final water content (w) and dry density (dd) along the block INF\_PELL1**

Mercury intrusion porosimetry tests were performed in each of these samples 3 months after dismantling of the cell (Campos *et al.* 2011a). Assuming that the percentage of pores not intruded in a clay corresponds entirely to the  $<7 \text{ nm}$  size (see section 3.2.1), an estimation of the percentage of micropores was computed. This was done for the samples and the percentage of each pore size recalculated. Figure 9 shows the corrected incremental and accumulated pore volume for the samples tested, with sample 1 being the closest to the hydration surface. Figure 10 and Table II show the pore size percentages recalculated and the mode of each pore size.

The percent of the porosity intruded by the mercury was fairly low (average 57%), this meaning that there was an important volume of pores with a size of less than  $7 \text{ nm}$  or not interconnected, that have been considered micropores. The percentage of them was hence on average 43%, with only sample 2 having less than 40% micropores. This sample is also the one with the highest percentage of macropores. Overall, the increase of water content implied an increase of microporosity and a decrease of mesoporosity percentage and size. On the contrary, the macropore size increased with water content, what could be an artefact due to the formation of cracks during exposure to room conditions upon dismantling.

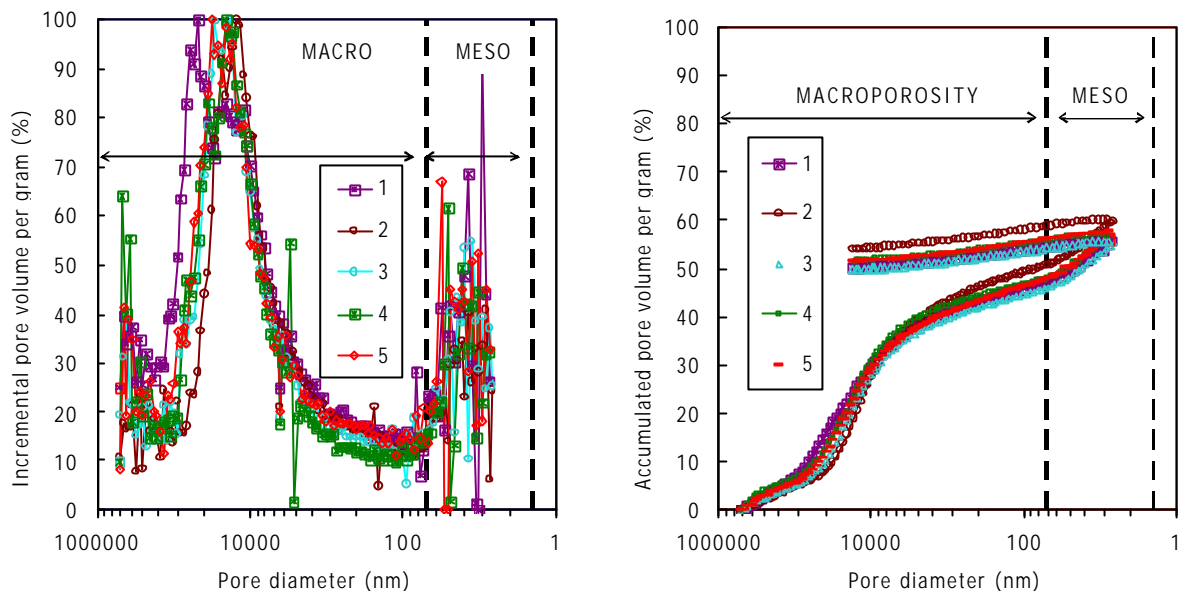


Figure 9: Mercury intrusion porosimetry results for samples of test INF\_PELL1

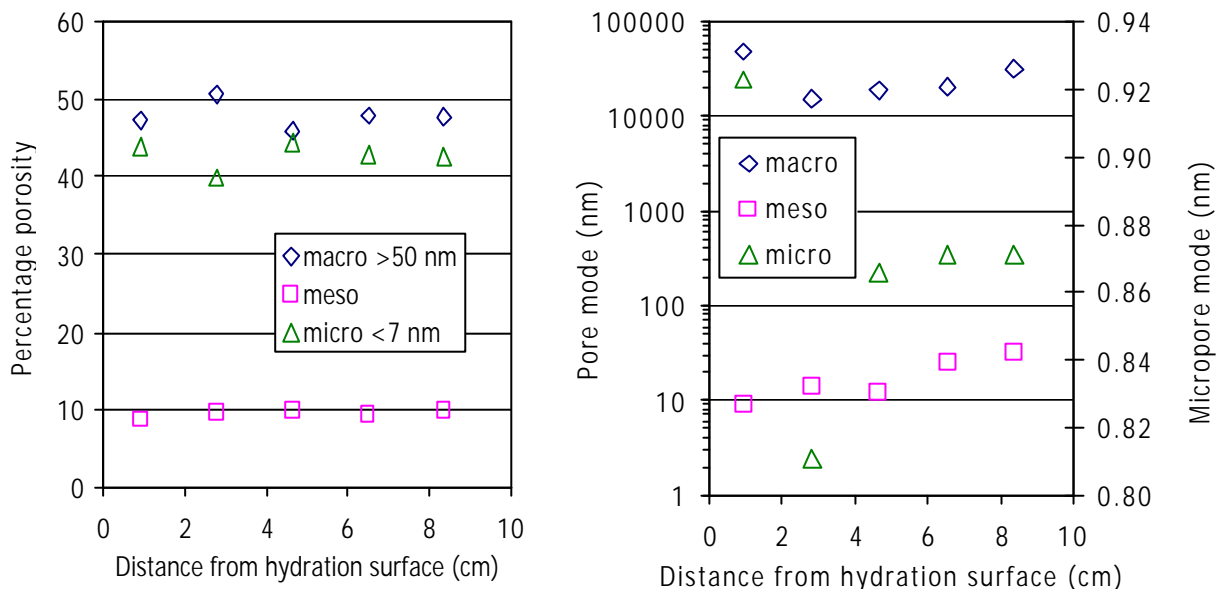
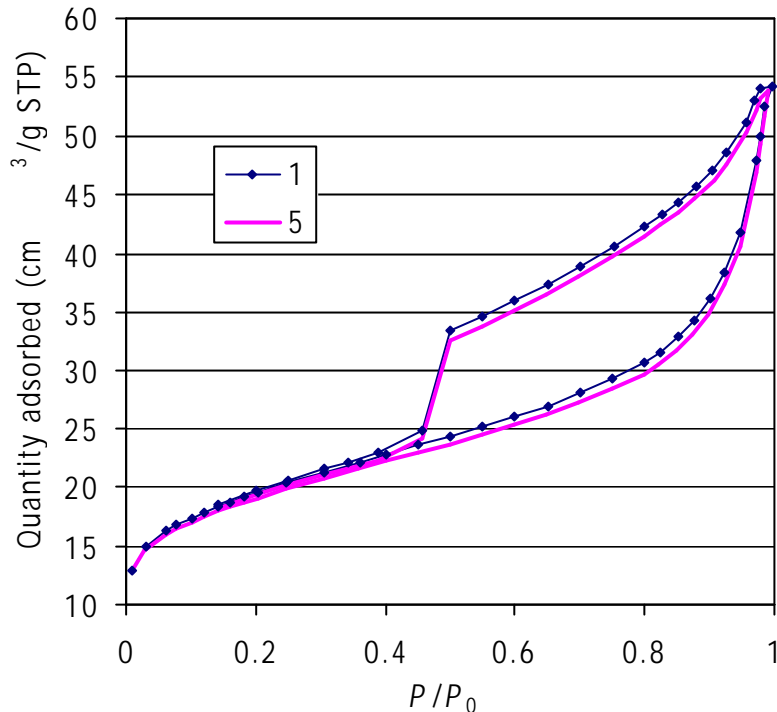


Figure 10: Pore size distribution of samples from test INF\_PELL1 (the micropore mode was obtained from the basal spacing measured by X-ray diffraction)

Table II: Final characteristics of samples from test INF\_PELL1, including MIP and X-ray diffraction results (sample 1 is the closest to the hydration surface)

Sample	$\rho_d$ (g/cm <sup>3</sup> )	w (%)	% intruded	% macro	Mode macro (nm)	% meso	Mode meso (nm)	% micro	d(001) (nm)
1	1.30	40.1	56	47	48179	9	9	44	1.903
2	1.34	38.7	60	51	15260	10	14	40	1.791
3	1.33	38.6	56	46	18795	10	12	44	1.846
4	1.32	38.9	57	48	20869	9	26	43	1.851
5	1.34	38.8	58	48	31679	10	32	42	1.851

The nitrogen adsorption isotherms measured in samples 1 and 5 are plotted in Figure 11. The BET specific surface areas obtained from them were 68.48 and 66.88 m<sup>2</sup>/g for samples 1 and 5, respectively (Campos *et al.* 2011a).



**Figure 11: Nitrogen adsorption isotherms of the samples closest (1) and farthest (5) from the hydration surface in test INF\_PELL1**

Figure 12 shows the X-ray diffraction patterns obtained for the 5 subsamples of the block immediately after dismantling. The intensity of the diffraction of sample 1 was clearly higher than that of the other samples, whereas the intensity of the diffraction of sample 2 was the lowest. From these diffraction patterns the basal spacing of the smectite could be determined, and the values obtained are included in Table II ( $d(001)$ ). An average value of 1.848 nm, corresponding to a 3-water layer hydration state, was obtained. Taking into account that these values correspond to the joint thickness of the TOT layer and of the interlayer, a micropore size was computed by subtracting to the basal spacing value the thickness of the TOT layer, which is 0.98 nm for the FEBEX bentonite, and the values obtained have been plotted in Figure 10.

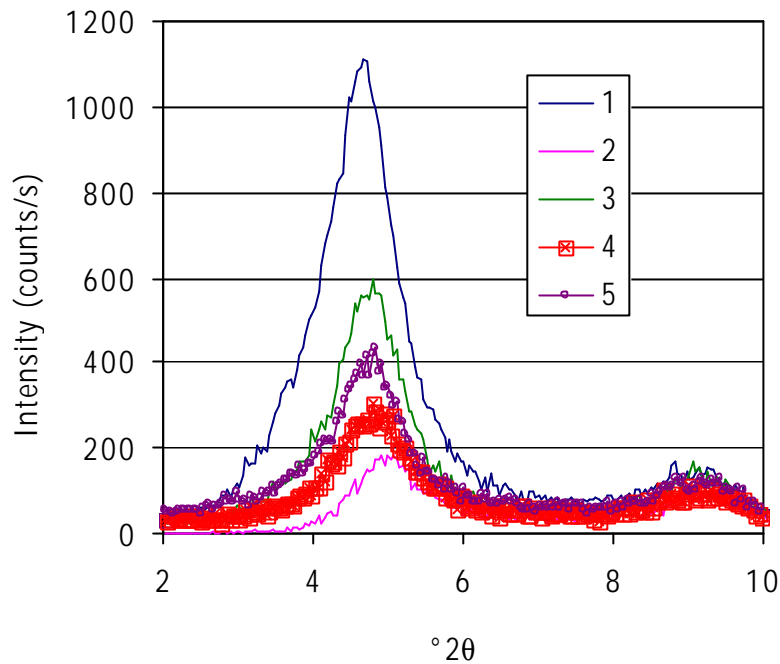


**Figure 12: X-ray diffraction patterns of untreated samples from test INF\_PELL1 (sample 1 is the closest to the hydration surface)**

## 4.2 TEST MGR13

This test was conducted in the large oedometer cell described in section 3.1.2. The pellets mixture prepared according to the curve shown in Figure 2 was directly compacted inside the cell at a nominal dry density of  $1.36 \text{ g/cm}^3$  with a nominal water content of 4.7% by applying a light uniaxial pressure. The block had an initial diameter of 10.0 cm and a height of 5.0 cm. Figure 13 shows the appearance of the pellets mixture after compaction.



**Figure 13: Appearance of sample for test MGR13 after compaction**

### 4.2.1 Online measurements

The test started in November 2006 and was dismantled in October 2009 after the permeability test phase. The saturation phase lasted 762 days, and the whole test lasted 1083 days. Saturation with deionised water was accomplished through the bottom surface of the sample according to the following sequence of events:

- Initially a 1.45-m water column was connected to the bottom of the sample, with the upper cell outlet open to atmosphere, so that for the air in the pores to be able to escape.
- After 287 h the upper outlet was closed.
- After 1491 h the upper outlet was again opened to atmosphere.
- After 1802 h the upper outlet was closed and the bottom inlet was connected to a pressure system set at 200 kPa.
- At an indeterminate time between 9595 and 11618 h the bottom inlet was again connected to the 1.45-m water column by mistake.
- After 11618 h the bottom inlet was connected again to the pressure system set at 200 kPa.
- After 13463 h the bottom inlet was again connected to the 1.45-m water column, and it could have been accidentally closed.
- After 14907 the bottom inlet to the cell is opened.

The evolution of water intake as measured by the volume change apparatus along with the vertical pressure developed during the test are shown in Figure 14, in which all the previously mentioned events have been indicated by vertical lines. During this saturation phase there was also a very slight decrease in dry density according to the LVDT measurement.

After 762 days saturation the water content according to the volume change apparatus would have been 45.0%. However, the final water content checked after dismantling was 37.1% (see next section), corresponding to a degree of saturation of 102%. Thus the water intake measurement by the volume change apparatus was at least a 24% overestimated, since the permeability measurement phase that followed saturation did probably result in a further increase of water content. The equilibrium swelling pressure was 1.5 MPa and was reached after approximately 80 days. The theoretical value corresponding to the granular FEBEX clay compacted to the same dry density is 1.15 MPa (Equation 3).

After the saturation phase the measurement of the hydraulic conductivity was undertaken. For that, the bottom inlet was connected to a pressure system applying a water pressure of 1200 kPa, while the upper outlet was connected to a pressure system applying a water pressure of 600 kPa. The hydraulic gradient applied was thus 1200. Two automatic volume change apparatuses measured the water exchange on top and bottom. The permeability test run for 321 days and the temperature during the measurement was  $22.9 \pm 2.6^\circ\text{C}$ .

The permeability value obtained from the water outlet was  $5.3 \cdot 10^{-13}$  m/s, whereas the value obtained from the water inlet was  $1.1 \cdot 10^{-12}$  m/s. This difference means that the water volume entering the sample was higher than the volume going out and consequently that some extra water was kept inside the sample during the permeability test. The theoretical permeability value at room temperature for a FEBEX granular sample compacted at the same dry density is, according to Equation 1,  $5.9 \cdot 10^{-13}$  m/s.

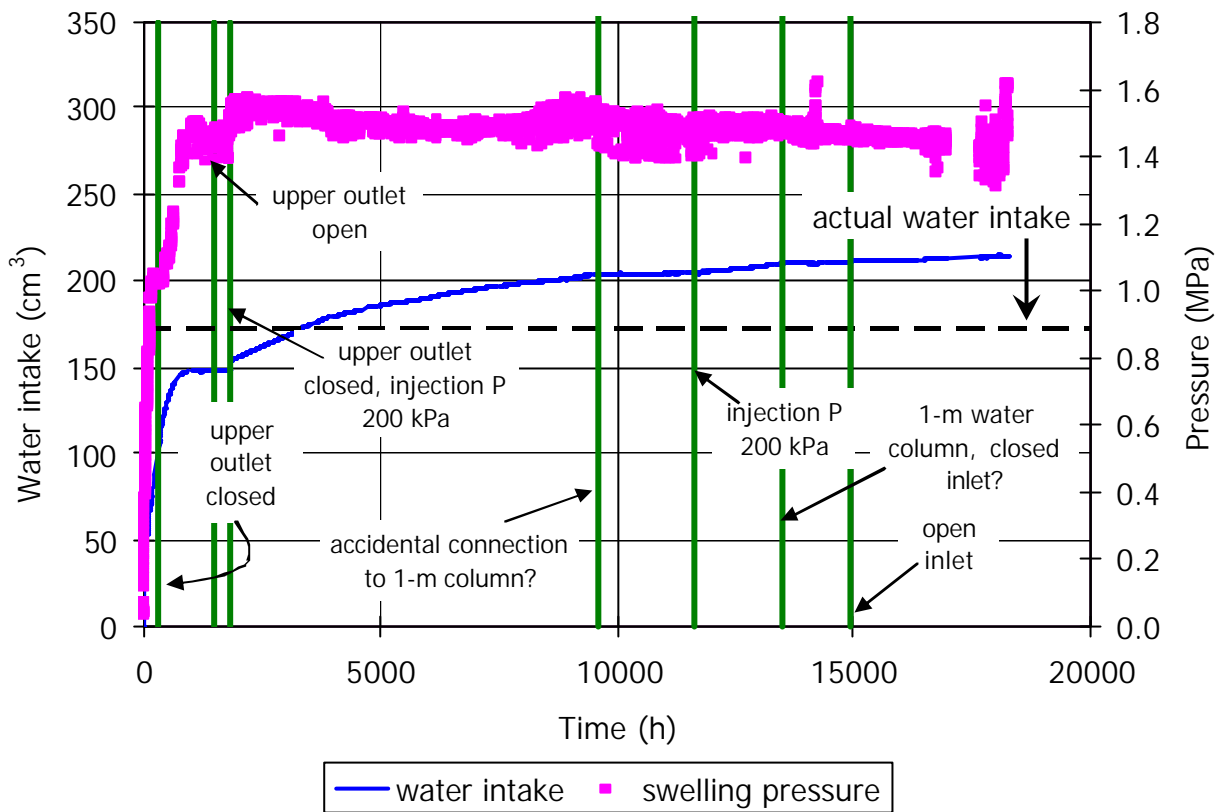


**Figure 14: Water intake and vertical pressure evolution during test MGR13**

#### 4.2.2 Post mortem analysis

After 1083 days operation (3 years) the oedometer cell was dismantled. The block was extracted, weighed and its dimensions measured. It was cut in three sections in which the different post mortem determinations were performed. Half of each subsample was used for dry density and water content determination, and the other half for the other post mortem determinations. The block displayed a perfectly saturated, homogeneous appearance and no pellets could be identified (Figure 15).



**Figure 15: Final appearance of the sample from test MGR13**

From the final dimensions measurement the dry density of the block was  $1.35 \text{ g/cm}^3$  and its final water content 37.1%, this would correspond to a degree of saturation of 102%. Figure 16 shows the measurements performed in the three equal levels in which the block was subsampled. The average water content measured in the subsamples was 36.7% and the dry density was  $1.34 \text{ g/cm}^3$ , lower than that calculated from the dimensions due to the fact that cutting for subsampling usually implies a slight decrease in dry density. The degrees of saturation computed from these values were slightly below 100%. The sample closest to the hydration surface (the bottom of the column) had the highest water content and lowest dry density.

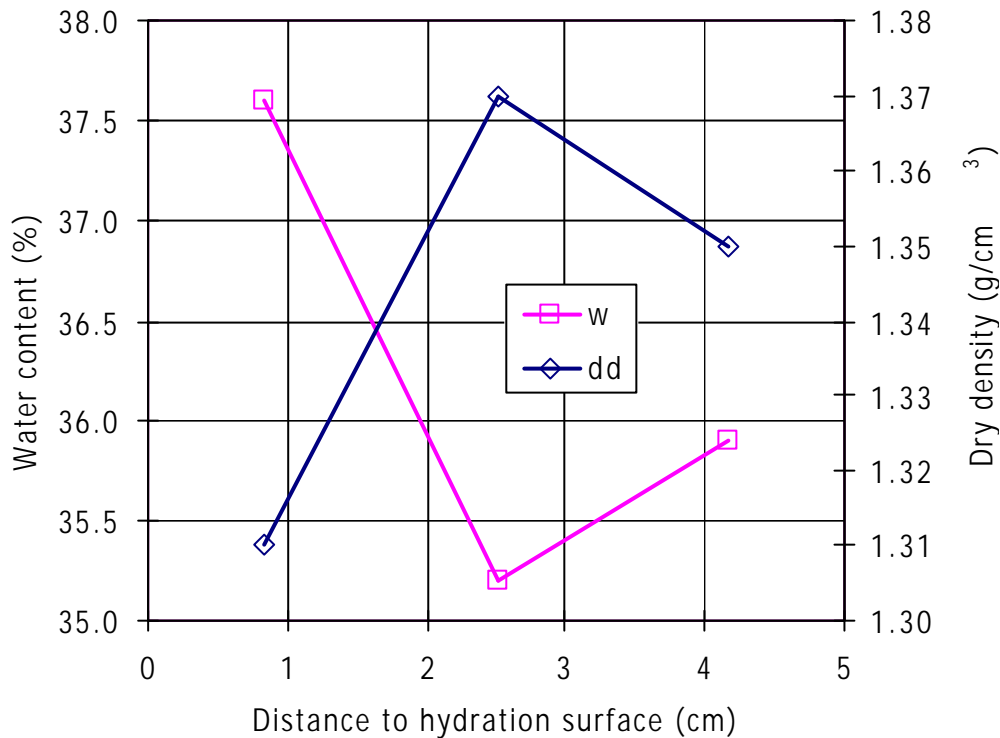


**Figure 16: Final water content (w) and dry density (dd) along the block MGR13**

Mercury intrusion porosimetry tests were performed in each of these samples previously lyophilised, although they had been kept wrapped in parffined foil 16 months after the test was dismantled (Campos *et al.* 2011b). This delay in the analysis could have implied changes in the microstructure, for which reason it is considered that these results must be interpreted cautiously. Figure 17 shows the corrected (taking into account the pore volume not intruded by mercury) incremental and accumulated pore volume for the samples tested, with sample 3 being the closest to the hydration surface. Figure 18 and Table III show the pore size percentages recalculated and the mode of each pore size. As in the case of the samples from test INF\_PELL1, the percent of the porosity intruded by the mercury was fairly low (average 58%), this meaning that there was an important volume of pores with a size of less than 7 nm or not interconnected, that have been considered micropores. The percentage of them was hence on average 42%.

Overall, the increase of water content implied an increase of the macropore mode and a decrease of mesoporosity percentage and size, as it was observed in the samples from test INF\_PELL1. Again, these observations could be related to the modifications of microstructure occurred upon storage prior to MIP analyses.

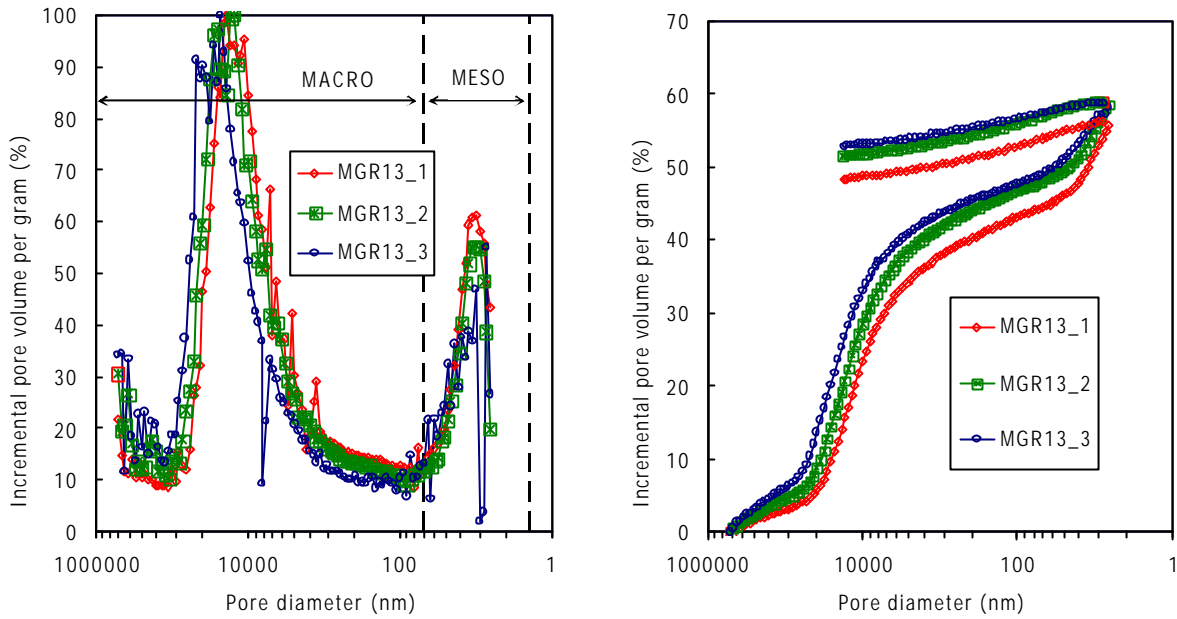


Figure 17: Mercury intrusion porosimetry results for samples of test MGR13 (sample 3 is the closest to the hydration surface)

Table III: Final characteristics of samples from test MGR13, including MIP and X-ray diffraction results (sample 3 is the closest to the hydration surface)

Sample	$\rho_d$ (g/cm <sup>3</sup> )	w (%)	% intruded	% macro	Mode macro (nm)	% meso	Mode meso (nm)	% micro	d(001) (nm)
1	1.35	35.9	56	44	18794	12	10	44	1.965
2	1.36	35.8	59	48	15252	11	10	41	1.957
3	1.31	38.3	59	49	23159	10	7	41	1.975

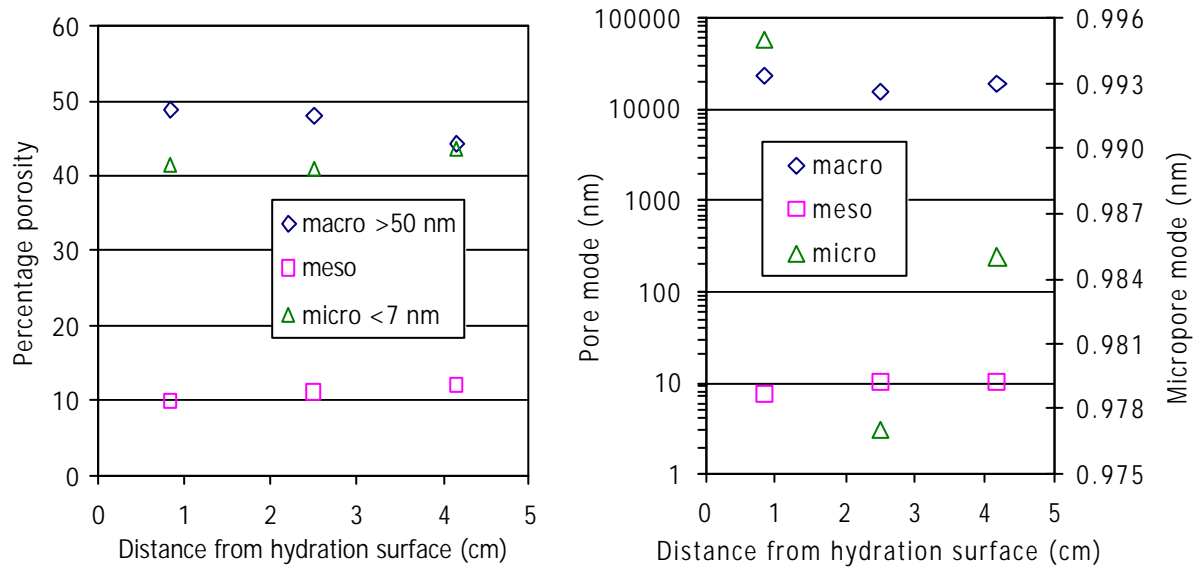


Figure 18: Pore size distribution of samples from test MGR13 (the micropore mode was obtained from the basal spacing measured by X-ray diffraction)

The nitrogen adsorption isotherms measured in the subsamples are plotted in Figure 19. The BET specific surface areas obtained from them were 69.27, 69.32 and 67.23 m<sup>2</sup>/g for samples 1 to 3, what means that it decreased with water content.

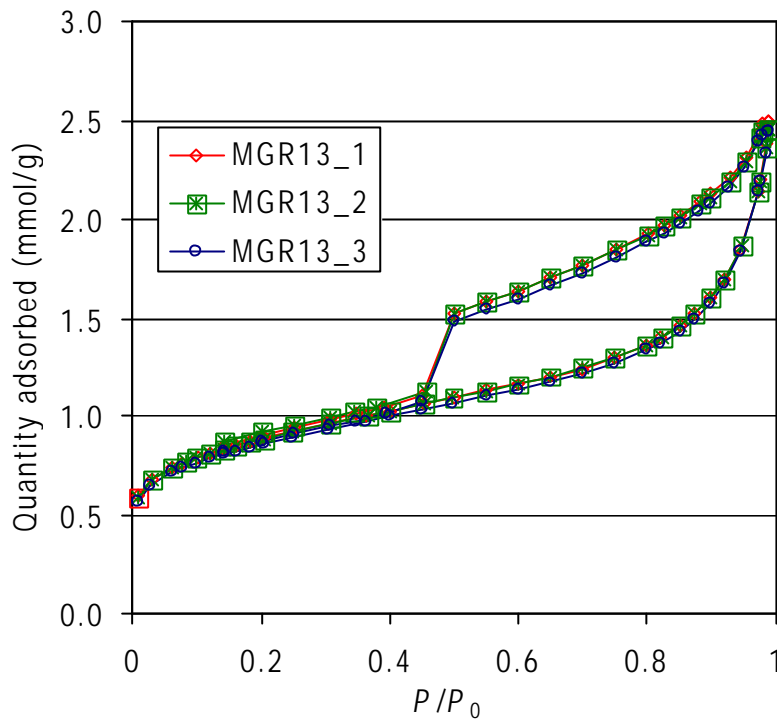


Figure 19: Nitrogen adsorption isotherms of the samples closest (3) and farthest (1) from the hydration surface in test MGR13

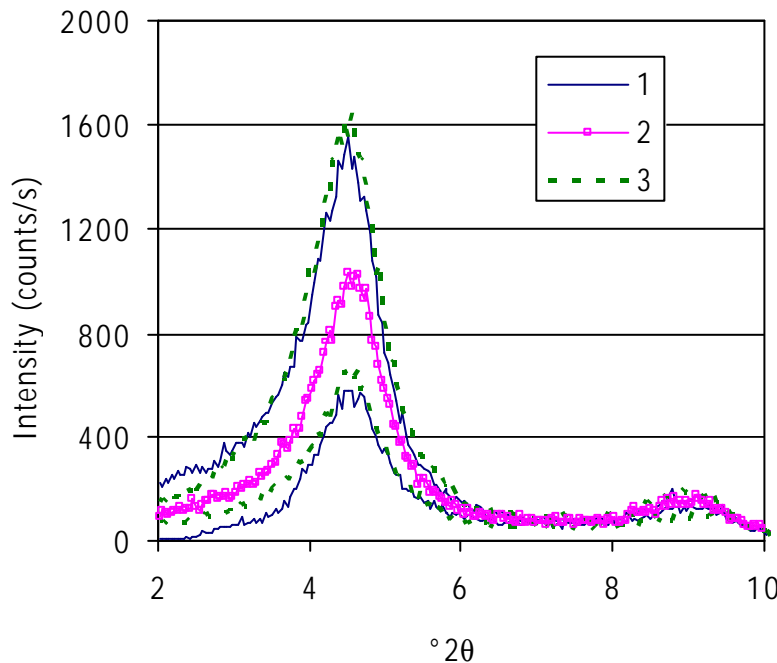


Figure 20: X-ray diffraction patterns of untreated samples from test MGR13 (sample 3 is the closest to the hydration surface)

Figure 20 shows the X-ray diffraction patterns obtained for the 3 subsamples of the block, with measurements on two different surfaces for samples 1 and 3. These analyses were performed immediately after dismantling. From these diffraction patterns the basal spacing of the smectite could be determined, and the values obtained are included in Table III ( $d(001)$ ). An average value of 1.966 nm, corresponding to a 3-water layer hydration state, was obtained. Taking into account that these values correspond to the joint thickness of the TOT layer and of the interlayer, a micropore size was computed by subtracting to the basal spacing value the thickness of the TOT layer, which is 0.98 nm for the FEBEX bentonite, and the values obtained have been plotted in Figure 18.

### 4.3 TEST MGR14

This test was conducted in the large oedometer cell described in section 3.1.2 with a 2-t load cell used to measure the vertical pressure developed upon saturation. The pellets mixture prepared according to the curve shown in Figure 2 was directly compacted inside the cell at a nominal dry density of  $1.36 \text{ g/cm}^3$  with a water content of 8.7% by applying a uniaxial pressure of 1.8 MPa. The water content had increased with respect to that the pellets had when they were received due to the long storage time and to the fact that the initial water content was much lower than the bentonite hygroscopic water content. The block had an initial diameter of 10.0 cm and a height of 5.0 cm.

#### 4.3.1 Online measurements

The test started in February 2010 and was dismantled in November 2010, the total duration being 265 days. Saturation with deionised water was accomplished through the bottom surface of the sample according to the following sequence of events:

- Initially a 1.45-m water column was connected to the bottom of the sample, with the upper cell outlet open to atmosphere, so that for the air in the pores to be able to escape.
- After 4823 h the bottom inlet was connected to a pressure system set at 600 kPa.
- After 5590 h the upper outlet was closed, since it was observed that water was oozing from it.

The evolution of water intake as measured by the volume change apparatus along with the vertical pressure developed during the test are shown in Figure 21, in which the previously mentioned events have been indicated by vertical lines. During the test there was also a slight decrease in dry density to values, according to the LVDT measurement, of  $1.35 \text{ g/cm}^3$ .

At the end of saturation the water content according to the volume change apparatus would have been 40.7%. However, the final water content checked after dismantling was 38.1% (see next section). Thus the water intake measurement by the volume change apparatus was a 9% overestimated. The equilibrium swelling pressure was 1.46 MPa and was reached after approximately 60 days. When the injection pressure was increased to 0.6 MPa, the pressure recorded by the load cell increased to 1.51 MPa, and the closing of the upper outlet led to a gradual increase up to values of 1.90 MPa. The theoretical value corresponding to the granular FEBEX clay compacted to the same dry density is 1.15 MPa (Equation 3).

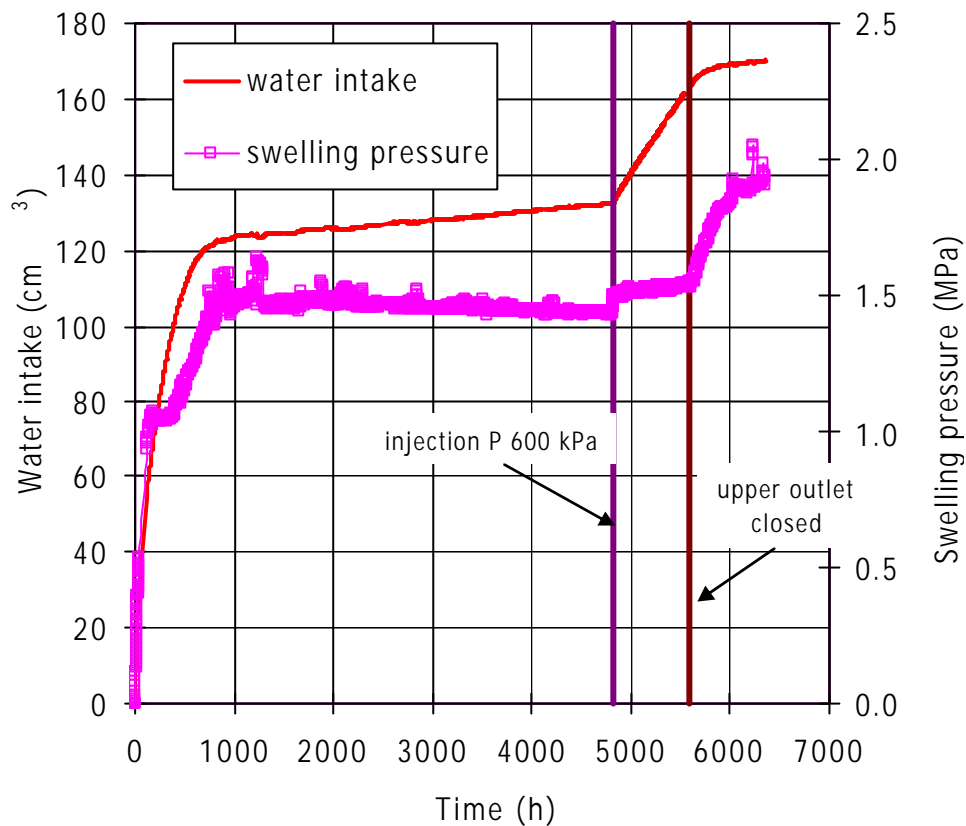


**Figure 21: Water intake and swelling pressure evolution during test MGR14**

#### 4.3.2 Post mortem analysis

After 265 days operation the oedometer cell was dismantled. The block was extracted, weighed and its dimensions measured. It was cut in three sections in which the different post mortem determinations were performed. Half of each subsample was used for dry density and water content determination, and the other half for the other post mortem determinations. The block displayed a perfectly saturated, homogeneous appearance and no pellets could be identified (Figure 22), although the external surface looked rougher than the MGR13 block (compare with Figure 15).

From the final dimensions measurement the dry density of the block was  $1.35 \text{ g/cm}^3$  and its final water content 38.1%, this would correspond to a degree of saturation of 104%. Figure 23 shows the measurements performed in the three equal levels in which the block was subsampled. The average water content measured in the subsamples was 37.2% and the dry density was  $1.35 \text{ g/cm}^3$ . The average degree of saturation computed from these values was 100%. The sample closest to the hydration surface (the bottom of the column) had the highest water content and lowest dry density.



Figure 22: Final appearance of the sample from test MGR14

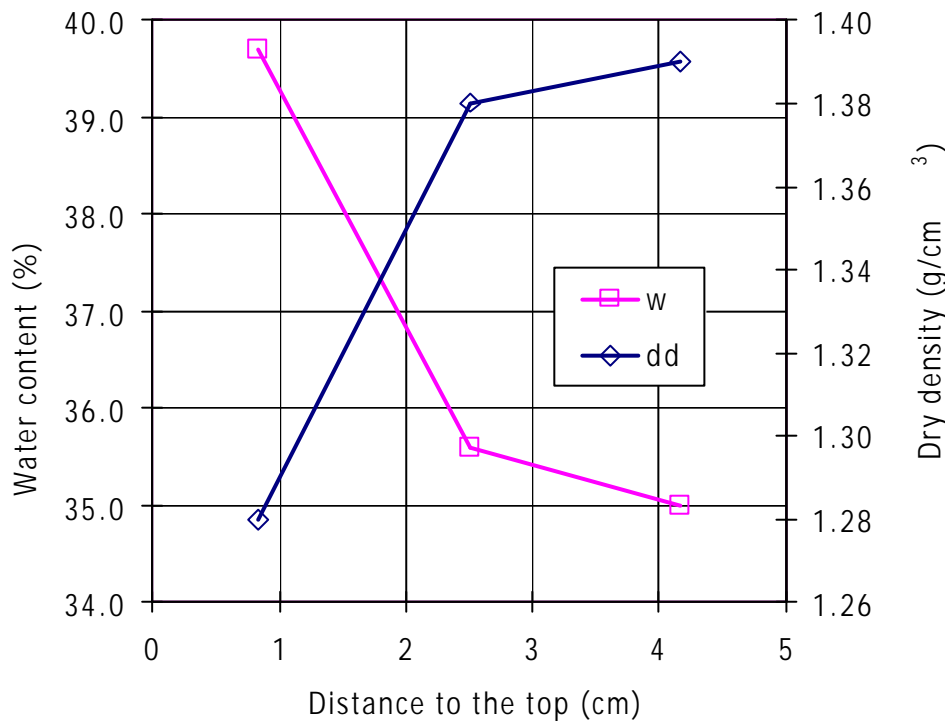


Figure 23: Final water content (w) and dry density (dd) along the block MGR14

Mercury intrusion porosimetry tests were performed in each of these samples previously lyophilised (Campos *et al.* 2011b), but they had been stored kept wrapped in paraffined foil for 5 months after the test was dismantled. This delay in the analysis could have implied changes in the microstructure, for which reason it is considered that these results must be interpreted cautiously. Figure 24 shows the corrected (taking into account the pore volume not intruded by mercury) incremental and accumulated pore volume for the samples tested, with sample 3 being the closest to the hydration surface. Figure 25 and Table IV show the pore size percentages recalculated and the mode of each pore size. Again, the percentage of the porosity intruded by the mercury was very low, even lower than in the other tests (average 45%), this meaning that there was an important volume of pores with a size of less than 7 nm or not interconnected, that have been considered micropores. The percentage of them was hence on average 55%, higher than for the other tests.

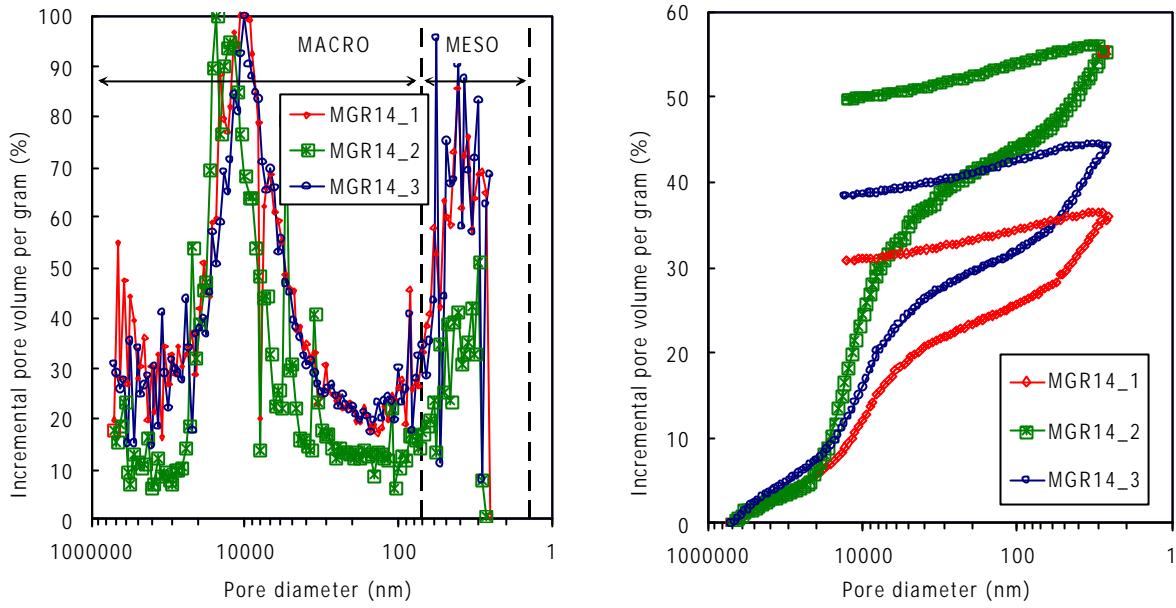


Figure 24: Mercury intrusion porosimetry results for samples of test MGR14 (sample 3 is the closest to the hydration surface)

Table IV: Final characteristics of samples from test MGR14, including MIP and X-ray diffraction results (sample 3 is the closest to the hydration surface)

Sample	$\rho_d$ (g/cm <sup>3</sup> )	w (%)	% intruded	% macro	Mode macro (nm)	% meso	Mode meso (nm)	% micro	d(001) (nm)
1	1.39	36.1	37	27	10017	10	32	63	1.830
2	1.38	35.6	55	46	23154	10	9	45	1.850
3	1.28	39.8	44	33	11119	11	17	56	1.860

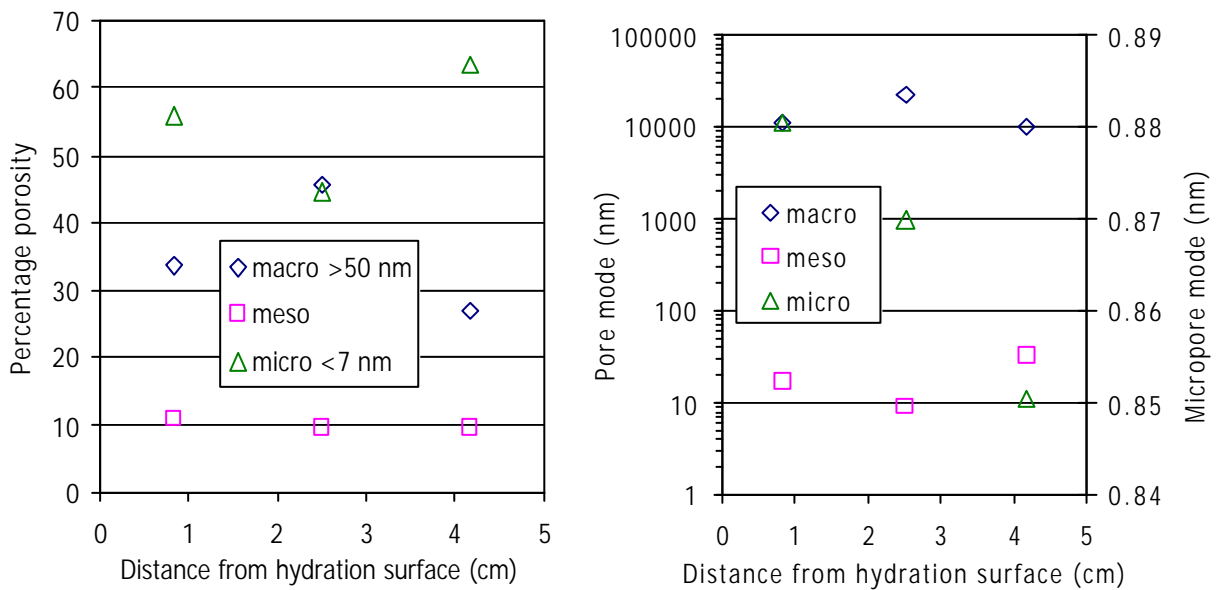


Figure 25: Pore size distribution of samples from test MGR14 (the micropore mode was obtained from the basal spacing measured by X-ray diffraction)

The nitrogen adsorption isotherms measured in the subsamples are plotted in Figure 26. The BET specific surface areas obtained from them were 67.57, 66.50 and 66.52 m<sup>2</sup>/g for samples 1 to 3.

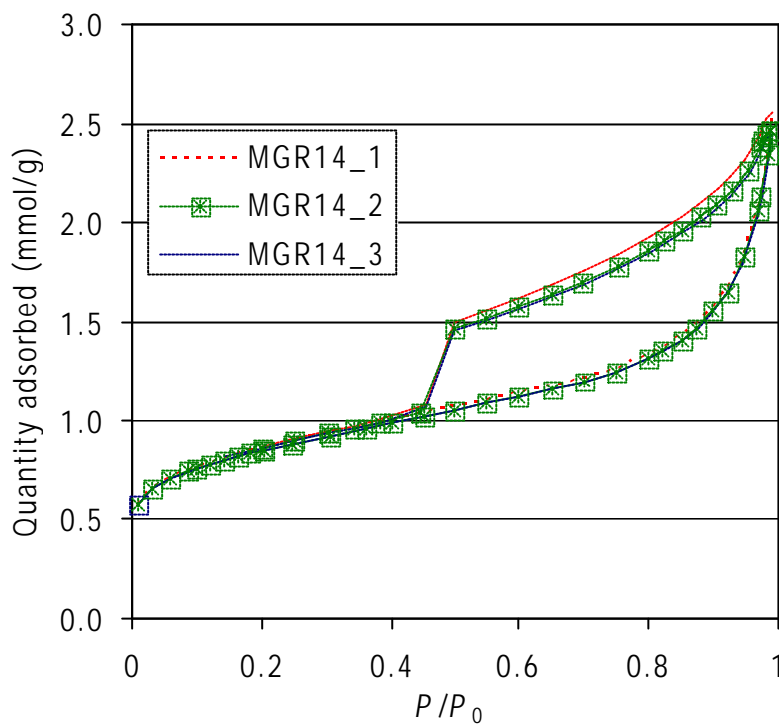


Figure 26: Nitrogen adsorption isotherms of the samples closest (3) and farthest (1) from the hydration surface in test MGR14

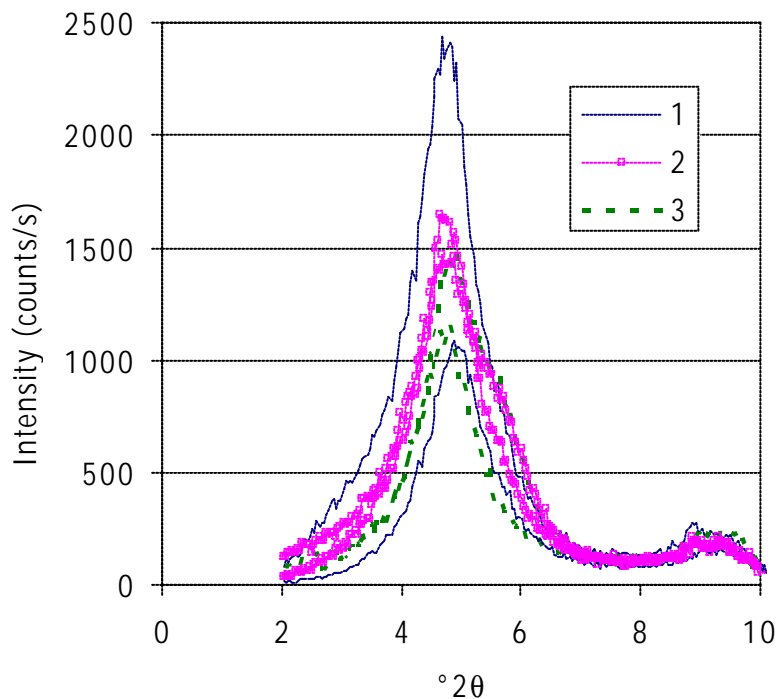


Figure 27: X-ray diffraction patterns of untreated samples from test MGR14 (sample 3 is the closest to the hydration surface)

Figure 27 shows the X-ray diffraction patterns obtained for the 3 subsamples of the block, with measurements on two different surfaces for each sample. These analyses were performed immediately after dismantling. From these diffraction patterns the basal spacing of the smectite could be determined, and the values obtained are included in Table IV ( $d(001)$ ). An average value of 1.847 nm, corresponding to a 3-water layer hydration state, was obtained. Taking into account that these values correspond to the joint thickness of the TOT layer and of the interlayer, a micropore size was computed by subtracting to the basal spacing value the thickness of the TOT layer, which is 0.98 nm for the FEBEX bentonite, and the values obtained have been plotted in Figure 25.

## 5 Summary and discussion

Three saturation tests under isochoric conditions were performed in cylindrical cells with the FEBEX pellets mixture used in the Mont Terri *in situ* EB experiment. The length of the cells was 5 or 10 cm. The nominal dry density of the mixture was low,  $1.36 \text{ g/cm}^3$ , as well as the water content (below 5%), for which reason it was not necessary to apply high compaction pressures to prepare the tests samples. Although in the *in situ* test Pearson synthetic water was used to saturate the buffer, deionised water was used in the laboratory tests. The water intake was measured in all the laboratory tests and, in two of them, the vertical stress developed upon saturation as well as the small vertical deformation allowed were also measured. In one of them a permeability test was run after saturation. After dismantling, several post mortem determinations were performed, mostly related to the analysis of the bentonite microstructure.

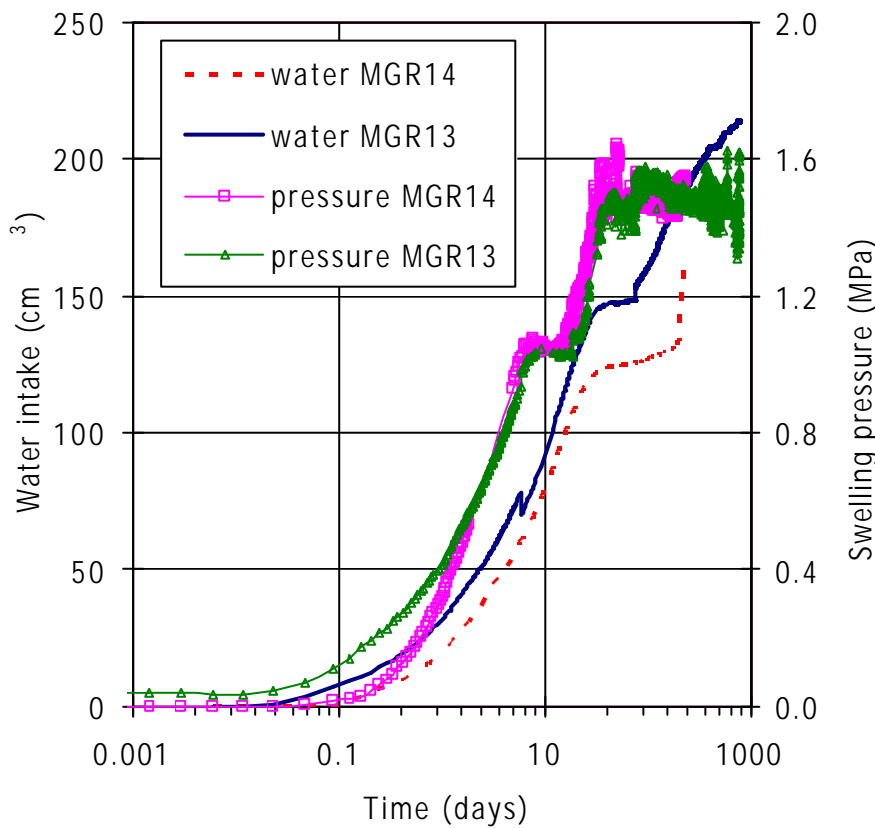
The online long-term measurement of the water intake was not accurate, and in the three tests the final water intake, as measured online, was overestimated. The water intake overestimation was 29%, 24% and 9%, increasing as the test was longer. Nevertheless, it was clear that most of the water was taken at the beginning of the experiment, approximately in the first 150 days for the 10-cm long cell, and in the first 30 days for the 5-cm long cells. Afterwards the water intake was very small and increased somewhat when the injection pressure was increased. No further water intake was recorded after 1200 days in the 10-cm long cell and after approximately 580 days in the 5-cm long cell.

With respect to the swelling pressure measurements, previous experience from tests performed in similar oedometers with bentonite had shown that the development of swelling pressure followed systematically a pattern in which the pressure increased sharply at the beginning of hydration, then stabilised or slightly decreased, and afterwards increased again, eventually reaching the equilibrium value. The following conclusions concerning swelling pressure development in bentonites were drawn (Imbert & Villar 2006):

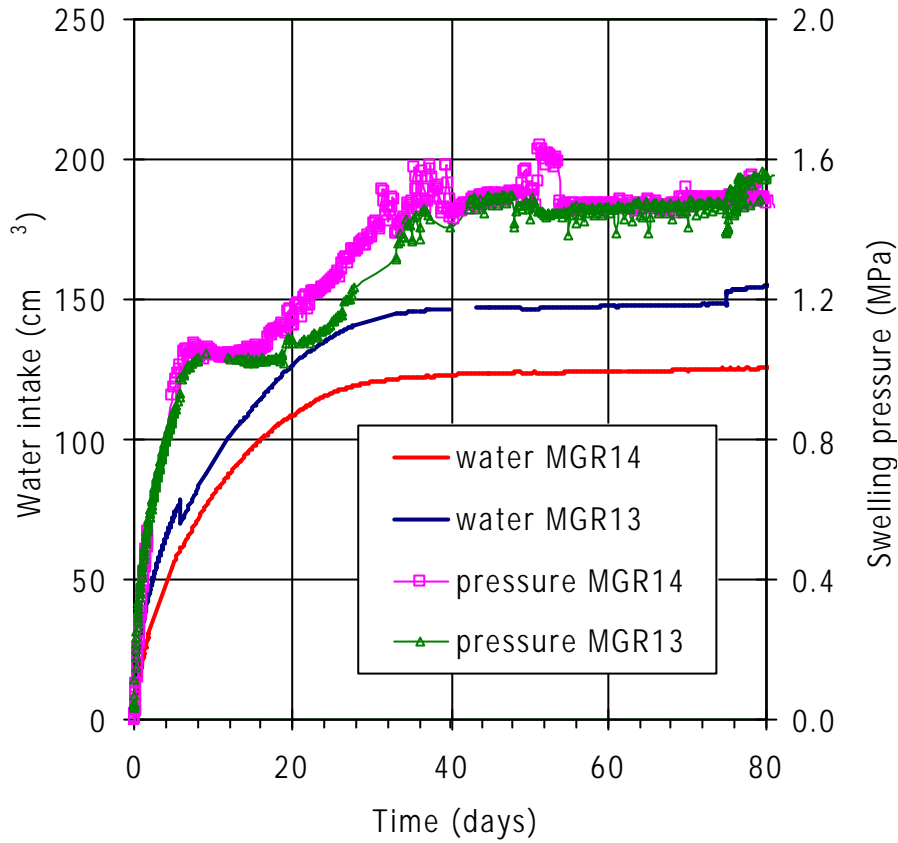
- 1 The increase/decrease/increase pattern of swelling pressure development appeared irrespective of dry density, size of sample and fabric.
- 2 The kinetics of the process depended on dry density, initial water content and size of the sample. This last fact should be taken into account when transferring laboratory test results to field conditions where scale and hydration paths are bound to be quite different (Gens *et al.* 2011).
- 3 The mixtures became homogeneous upon saturation, with swelling pressure and hydraulic conductivity similar to those of compacted powder of the same dry density.
- 4 Scale effect: the swelling pressure obtained in large oedometers tended to be higher.

Figure 28 compares the results obtained in the two tests performed in oedometer. The swelling pressure development pattern and rate as well as the intermediate and final equilibrium values were similar, despite the fact that different load cells were used in each test. This gives confidence in the results obtained. The water intake rate was also similar in both tests, although the actual values were inaccurate. The initial sharp increase in swelling pressure coincided with the high initial water intake rate. After just 7 days the first pressure equilibrium value – 1 MPa – was reached and kept constant until day 16-18, when pressure started to increase again and the water intake rate to soften. The final equilibrium swelling pressure value – 1.5 MPa – was reached after approximately 36 days and the water intake was comparatively very small afterwards (Figure 29).

These swelling pressure values have been plotted in Figure 30 as a function of the final dry density as computed from the strain online measurements (which were only slightly lower than the initial dry density due to the small vertical deformation allowed). The experimental fitting for the FEBEX granular bentonite (<5 mm) obtained from shorter tests performed in small standard oedometers is also included in the Figure (Equation 3). The results obtained for the pellets mixture lay in the upper limit of the theoretical values. As mentioned above, the swelling pressure tended to be higher when it was determined in large samples.



**Figure 28: Evolution of swelling pressure and water intake in tests MGR13 and MGR14**



**Figure 29: Measurement of the initial phase of tests MGR13 and MGR14 (the water injection pressure in this phase was 10 kPa)**

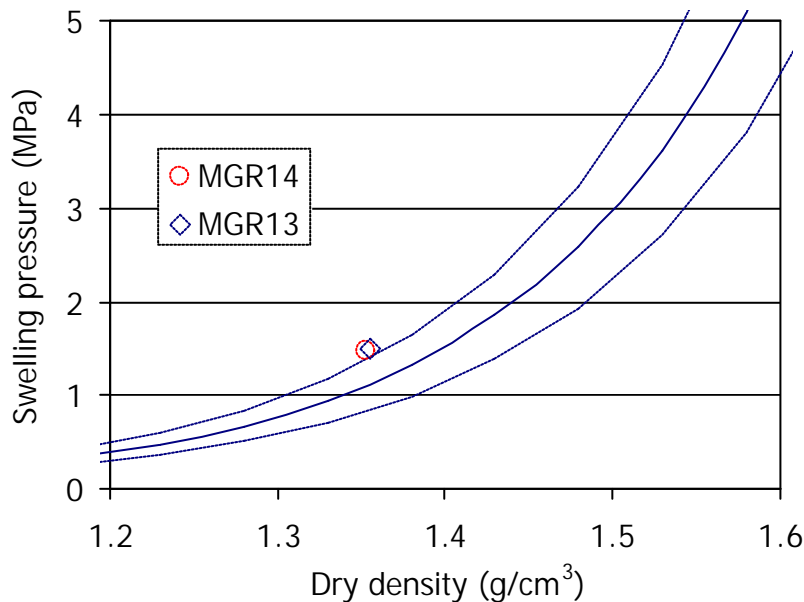


**Figure 30: Swelling pressure values measured in the tests performed in the large oedometer and theoretical fitting for FEBEX granular bentonite (Equation 3)**

In the framework of the project RESEAL I (Volckaert *et al.* 2000), several swelling pressure tests were performed in the same oedometer equipment with FEBEX bentonite. In one of them the granular clay (<5 mm) was used and in the two others a pellets-based mixture was used. The

pellets were different from those of the EB experiment, they were manufactured by Sahut-Conreur (Raismes, France) and were bigger, wetter and with a lower dry density (around 1.84 g/cm<sup>3</sup>). The characteristics of those tests are summarised in Table V.

**Table V: Characteristics of the swelling pressure tests performed in the large oedometer during RESEAL I and for the EB project**

Reference	Fabric	Height (cm)	Dry density (g/cm <sup>3</sup> )	Initial w (%)	Saturation
MGR1	granular <5 mm	10	1.50	12.6	Both surfaces, 0.6 MPa
MGR2	pellets/granulate 62/38	10	1.40	11.0	Both surfaces, 0.6 MPa
MGR3	pellets/powder 70/30	10	1.44	13.6	Bottom, water column/0.6 MPa
MGR13	EB mixture	5	1.35	4.7	Bottom, water column
MGR14	EB mixture	5	1.35	8.7	Bottom, water column

The evolution of pressure in these tests is plotted in Figure 31. The rate of pressure development is clearly quicker in the tests in which a high injection pressure was applied from the beginning (MGR1 and MGR2). Indeed the final vertical pressure value depended mainly on dry density, but also on the water injection pressure, since the load cell recorded both the mechanical pressure developed by the clay and the water pressure. It is difficult to tell apart the contribution of each of them, which may have changed as the clay saturated. In test MGR3, it was observed that when the water injection was stopped, the pressure value registered by the load cell decreased instantly 0.3 MPa, and afterwards dissipated slowly (Villar & Martín 1998). The water intake was also faster in the tests in which a high injection pressure was applied, with most of the water entering in a few hours. This, along with the initially homogeneous fabric of test MGR1, could be the reasons why the pressure increase/stabilisation/increase pattern was not observed in this test. In tests with FoCa bentonite (Imbert & Villar 2006) it was checked that –when saturation was performed under very low water injection pressure– the swelling pressure development was faster the lower the dry density and the shorter the bentonite sample. The results in Figure 31 show the opposite, and the cause could be the higher injection pressure applied in tests MGR1 and MGR2, which seems to have also an influence on the swelling pressure development kinetics, at least for dry densities below 1.5 g/cm<sup>3</sup>.

The hydraulic conductivity values determined after saturation in tests MGR3 and MGR13 have been plotted in Figure 32 along with the experimental relationship between hydraulic conductivity and dry density determined for the compacted granular clay (Equation 1) and for pellets mixtures (Equation 4) in different laboratories. The value for test MGR3 was obtained after saturation applying hydraulic gradients of 1400 and 2400. The values obtained in the large oedometer agree with the fitting obtained at CIEMAT (Equation 1), what would indicate that the initial fabric of the material (granulate or pellets) does not affect the hydraulic conductivity of the saturated material.

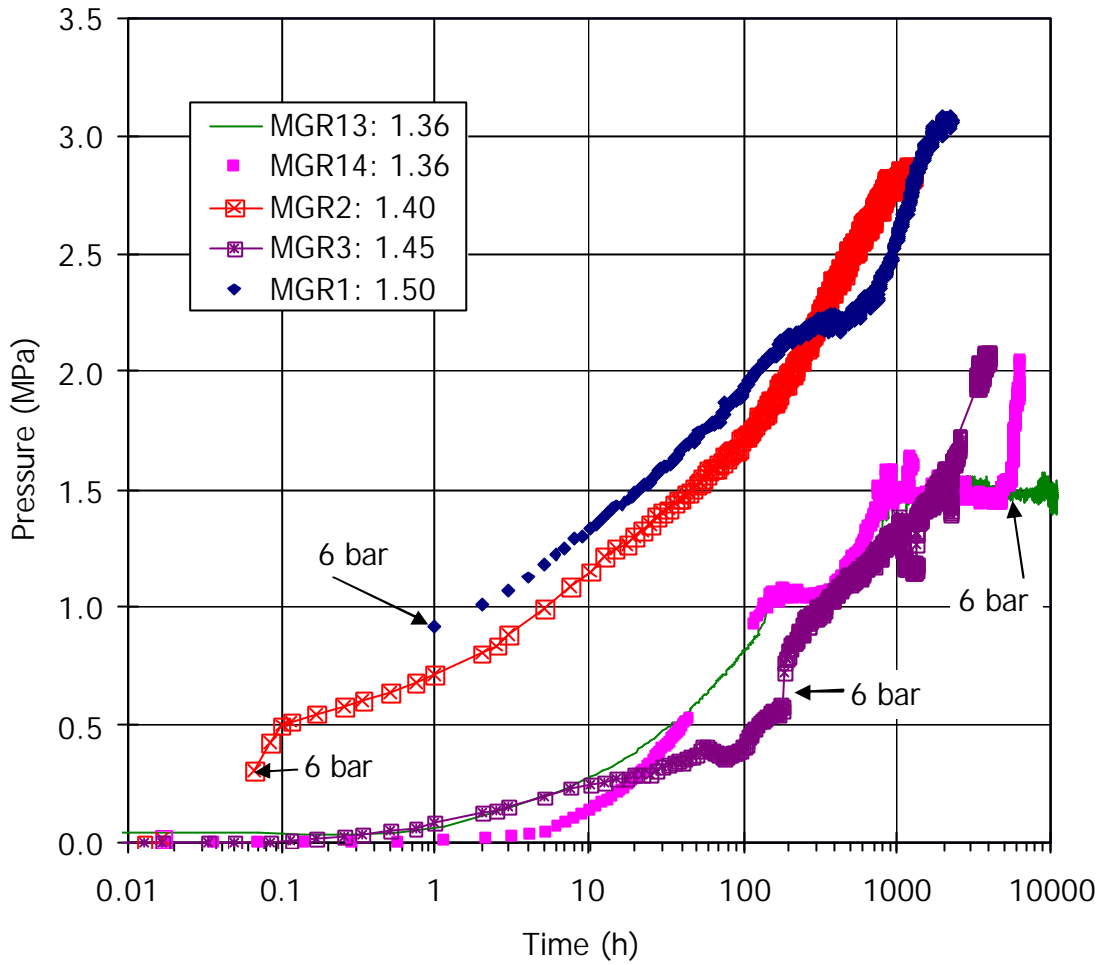


Figure 31: Evolution of vertical pressure in tests performed in the large oedometer with FEBEX bentonite in the framework of RESEAL and EB projects (see Table V for details)

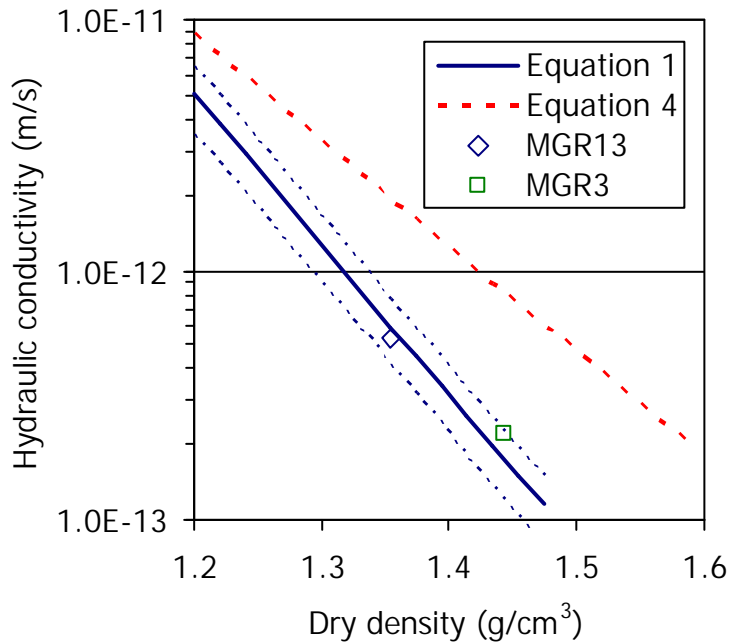


Figure 32: Hydraulic conductivity measured in tests MGR3 and MGR13 and theoretical fittings for FEBEX granular bentonite (Equation 3) and pellets mixtures (Equation 4)

The dismantling of the cells, which included the weighing, measuring and subsampling of the clay blocks, allowed to check the actual final conditions of the pellets mixture. At the end of the three tests the bentonite looked homogeneous, saturated and no pellets could be told apart. Direct observations of the hydration process of a pellets/powder mixture were obtained by van Geet *et al.* (2005) using microfocus X-ray computed tomography. They observed the following phases:

1. at the initial state there was a clear difference in density between pellets and powder;
2. during hydration, the density of the pellets reduced (swelling) while the density of the powder rose because of both soil compression and water content increase; the changes moved gradually from the hydration surface to the opposite surface following the progress of hydration;
3. an apparently homogeneous specimen was obtained at the end of the test.

Upon dismantling the water content along the blocks was uniform, except for the sections closest to the hydration surface, which had significant higher water contents, especially in the tests in which a high injection pressure was applied (tests MGR). These sections had also clearly lower dry densities, whereas the rest of the mixture had similar dry densities (Figure 33). This could indicate that the swelling of the bentonite closest to the hydration surface led to an irreversible deformation and, despite the fact that at least two of the tests run until no more water intake was recorded, the water content and the dry density near the hydration surface remained different than in the rest of the bentonite.

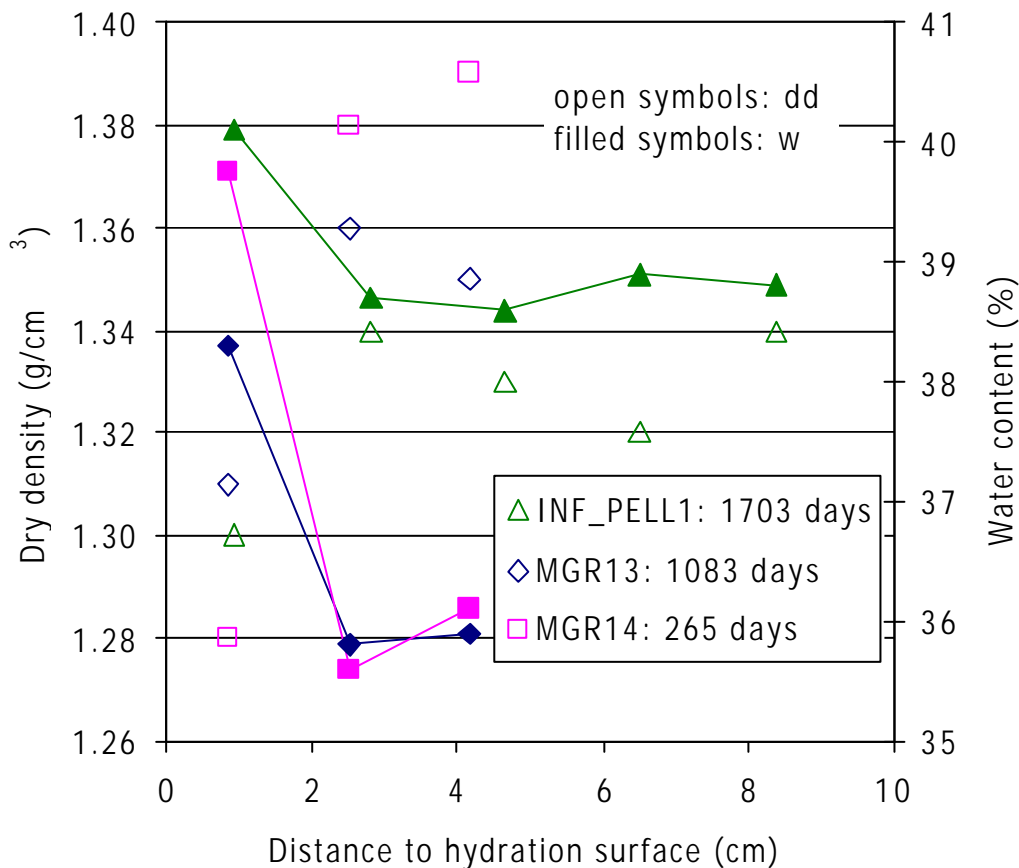
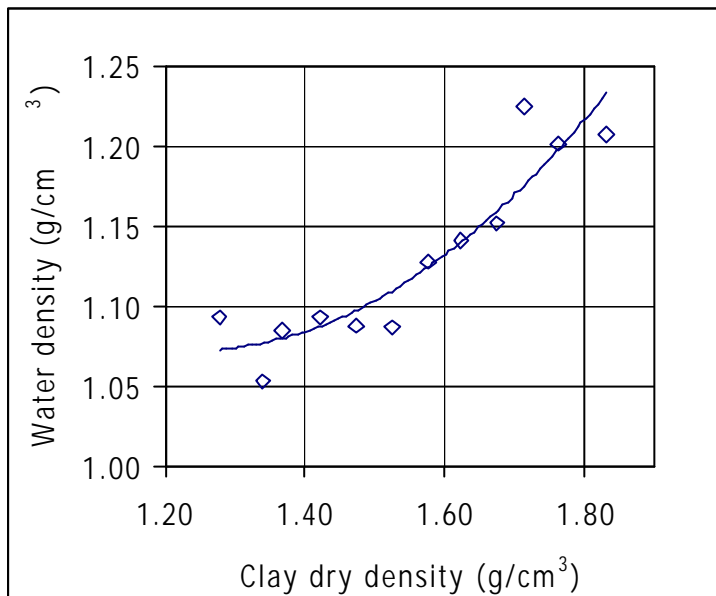


Figure 33: Final dry density (dd) and water content (w) along the bentonite columns

The final degrees of saturation of the bentonite columns, computed by taking a water density of  $1.00 \text{ g/cm}^3$ , were between 102 and 104% for dry densities of between  $1.33$  and  $1.35 \text{ g/cm}^3$ . Considering that this small deviation with respect to the 100% value was due to the change in interlayer water density, a value of pore water density of  $1.02$ - $1.04 \text{ g/cm}^3$  would be obtained, which is slightly below the values reported by Villar (2002) for FEBEX bentonite for similar dry densities. Consequently, it is not considered that the computation of the water intake in the laboratory and *in situ* tests could be affected by the changes in pore water density.



**Figure 34: Pore water density as a function of FEBEX bentonite dry density as proposed by Villar (2002)**

The analysis of the pore size distribution results obtained by MIP has to be made taking into account that they were performed several months after the dismantling of the tests (16 months in the case of test MGR13). Although the samples were preserved against moisture changes, the microstructure could have been modified because of the changes in the stress state and of water redistribution. When the three tests are jointly examined no distinctive features of the pore size distribution become patent, maybe because all the samples had the same initial fabric and, despite the different duration of the tests, similar final dry densities and water contents. As it is usual in compacted bentonite, the percentage of pores intruded by the mercury, as computed from the difference between the actual dry density of the samples and that measured by the porosimeter, was low, usually between 50 and 60%. Most of the porosity belonged to the micropore size, considered here as those pores not intruded by mercury (of diameter  $<7 \text{ nm}$ ). The macroporosity percentage ( $>50 \text{ nm}$ ) was also important, what could be an artefact due to the formation of cracks during exposure to room conditions upon dismantling or to the expansion of the microstructure during storage. The mode of the macropores was  $21 \pm 11 \mu\text{m}$  and tended to decrease with the dry density. The mesopore size, with a mode of  $16 \pm 9 \text{ nm}$ , was the less represented.

Since the micropore size cannot be explored with the MIP technique, the measurement of the basal spacing by X-ray diffraction, which can partly supply this information, was undertaken. Also the BET specific surface area was measured by nitrogen adsorption.

The values obtained for the two parameters in the three tests are plotted in Figure 35 as a function of the distance from the hydration surface, which in turn is related to the water content. In each test the basal spacing increased with the water content, but all the values

obtained indicated the formation of the 3-layer hydrate. What is striking is that, despite the fact that the average final water content and dry density in all the tests were not very different, the basal spacings measured in test MGR13 were considerably higher. The main differences among the tests was the duration, which was much shorter for test MGR14, and that hydraulic conductivity was determined after saturation applying a pressure of 1.2 MPa in test MGR13, whereas the maximum water pressure applied in the other two tests was 0.6 MPa. The application of a higher water pressure could be the reason for the higher basal spacings of the samples from this test. The time of contact with water has also been considered by several authors to have an influence on the basal spacing, which would be higher the longer the equilibration time (Villar *et al.* 2012).

The specific surface area was similar for all the samples, with an average value of  $68 \pm 1$  m<sup>2</sup>/g and no particular trend along the bentonite blocks.

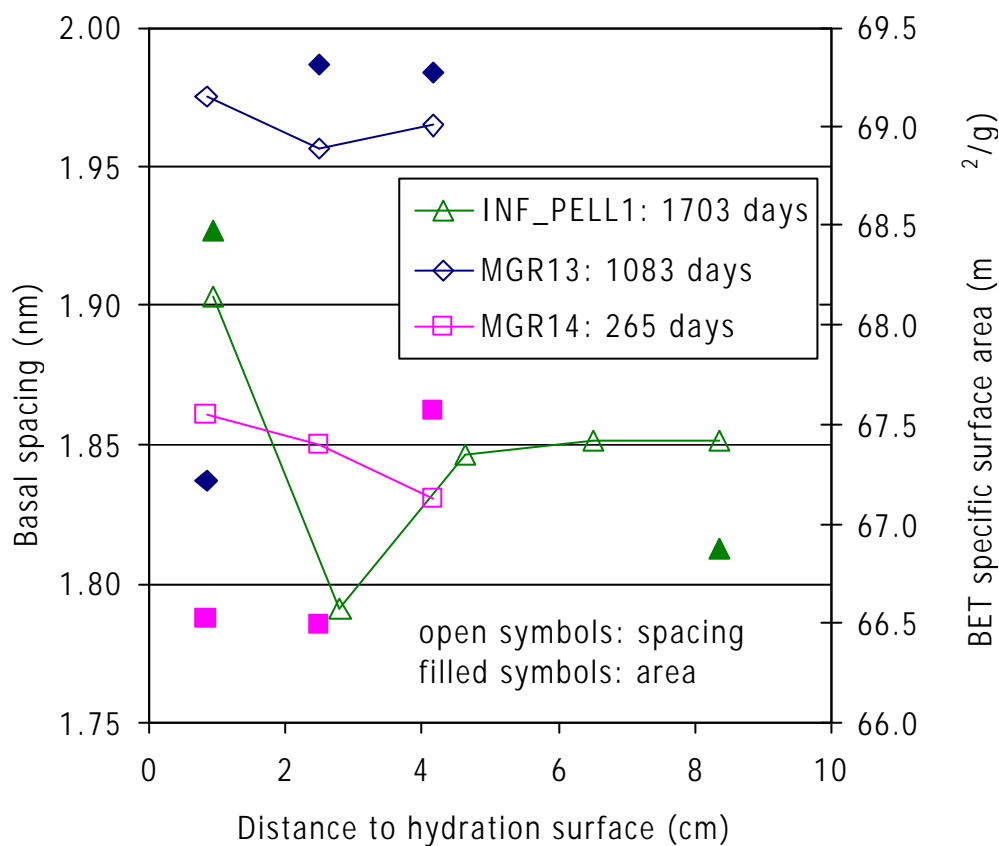


**Figure 35: Basal spacing and BET specific surface area measured at the end of the tests in bentonite subsamples**

## Conclusions

Three saturation tests under isochoric conditions were performed in cylindrical cells with the FEBEX pellets mixture used in the Mont Terri *in situ* EB experiment.

Most of the water was taken at the beginning of the experiments, but this initial phase took longer the longer the sample. Afterwards the water intake was very small and increased somewhat when the injection pressure was increased. No further water intake was recorded after 1200 days in the 10-cm long cell and after approximately 580 days in the 5-cm long cell.

The development of swelling pressure followed a pattern in which the pressure sharply increased at the beginning of hydration, then stabilised, and afterwards increased again, eventually reaching the equilibrium value when most of the water had already been taken. Previous investigations systematically showed this pattern when saturating bentonite samples under isochoric conditions, irrespective of dry density, size of sample or fabric, with the actual kinetics of the process depending on the dry density, initial water content and size of the sample. The comparison of the tests presented here with tests performed with the FEBEX bentonite in previous investigations showed that the water injection pressure is also a determinant factor in the water intake and pressure development rate.

The mixtures became homogeneous upon saturation, with swelling pressure and hydraulic conductivity similar to those of compacted granular samples of the same dry density. The swelling pressure obtained for the pellets mixture – 1.5 MPa – lay in the upper limit of the theoretical value for compacted granular FEBEX bentonite. A certain scale effect was noticed in previous investigations, the swelling pressure tended to be higher when it was determined in large samples.

Upon dismantling the water content and dry densities along the blocks was uniform, except for the sections closest to the hydration surface, which had significantly higher water contents and lower dry densities, especially in the tests in which a high injection pressure was applied. Since the tests run until no more water intake was recorded, this could indicate that the swelling of the bentonite closest to the hydration surface led to an irreversible deformation and water content.

It is not considered that the computation of the water intake in the laboratory and *in situ* tests could be affected by the changes in pore water density, since this is close to  $1.0 \text{ g/cm}^3$  due to the low average dry density of the bentonite.

The analysis of the microstructure of the mixture at the end of the tests showed that most of the porosity was of a diameter smaller than 7 nm. The macroporosity percentage (>50 nm) was also important, what could be an artefact due to the formation of cracks during exposure to room conditions upon dismantling or to the expansion of the microstructure during storage. The mode of the macropores was  $21 \pm 11 \text{ } \mu\text{m}$  and tended to decrease with the dry density. The mesopore size, with a mode of  $16 \pm 9 \text{ nm}$ , was the less represented.

The basal spacing of the smectite, measured by Xray diffraction, increased with the water content, with all the values indicating the formation of the 3-layer hydrate. The application of a higher water injection pressure in one of the tests resulted in higher basal spacings, which is something not previously remarked. The specific surface area was similar for all the samples, with an average value of  $68 \pm 1 \text{ m}^2/\text{g}$  and no particular trend along the bentonite blocks.

When transferring these laboratory test results to field conditions, where scale and hydration paths are quite different, the scale effect should be taken into account, and also the geochemistry of the system, since in the *in situ* test Pearson synthetic water was used to saturate the buffer, whereas deionised water was used in the laboratory tests. Lower swelling pressures and higher hydraulic conductivities are to be expected when saline water is used as saturating fluid.

## Acknowledgements

The research leading to these results received funding from the European Atomic Energy Community's Seventh Framework Programme (FP7/2007-2011) under Grant Agreement n°249681, the PEBS project. This work was additionally financed by ENRESA through a CIEMAT-ENRESA General Agreement. The laboratory work was performed by Ramón Campos and Juan Aroz, at CIEMAT. The X-ray diffraction tests were performed by Luis Gutiérrez-Nebot from CIEMAT and the mercury intrusion porosimetry and nitrogen adsorption tests in the CIEMAT laboratory run by Dr. Rocío Campos.

## References

- CAMPOS, R., GONZÁLEZ, A.M. AND BARRIOS, I. 2011a. Ensayo de infiltración en pellets: porosidad y superficie específica. *Informe Técnico CIEMAT/DMA/2G210/7/11*. CIEMAT, Madrid, 9 pp.
- CAMPOS, R., GONZÁLEZ, A.M. AND BARRIOS, I. 2011b. Ensayos MGR13 y MGR14: Análisis de la porosidad y superficie específica. *Informe Técnico CIEMAT/DMA/2G210/2/11*. CIEMAT, Madrid, 11 pp.
- DELAGE, P. & LEFEBVRE, G. 1984. Study of the structure of a sensitive Champlain clay and its evolution. *Can. Geotech. J.* 21(1): 21-35.
- ENRESA 2005. "Engineered barrier emplacement experiment in Opalinus Clay for the disposal of radioactive waste in underground repositories" Final Report. *Publicación Técnica ENRESA 02/05*. Madrid, 101 pp.
- GENS, A.; VALLEJÁN, B.; SÁNCHEZ, M.; IMBERT, C.; VILLAR, M.V. & VAN GEET, M. 2011. Hydromechanical behaviour of a heterogeneous compacted soil: experimental observations and modelling. *Géotechnique* 61(5): 367-386.
- HOFFMANN, C. 2005. Caracterización hidromecánica de mezclas de pellets de bentonita. Estudio experimental y constitutivo. *PhD Thesis*. Universitat Politècnica de Catalunya, Barcelona, 387 pp.
- IMBERT, CH. & VILLAR, M.V. 2006. Hydro-mechanical response of a bentonite pellets/powder mixture upon infiltration. *Applied Clay Science* 32: 197-209.
- PEARSON F. 1998. Artificial waters for use in laboratory and field experiments with Opalinus Clay. *Paul Scherrer Institut TM 44-98-08*
- SING, K.S.W., EVERETT, D.H., HAUL, R.A.W., MOSCOU, L., PIEROTTI, R.A., ROUQUÉROL, J., SIEMIENIEWSKA, T. 1985. Reporting physisorption data for gas/solid systems with special reference to the determination of surface area and porosity. *Pure & Appl. Chem.* 57(4): 603-619. IUPAC.
- UNE 7045(1952): Determinación de la porosidad de un terreno.
- VAN GEET, M., VOLCKAERT, G., ROELS, S., 2005. The use of microfocus X-ray computed tomography in characterising the hydration of a clay pellet/powder mixture. *Appl. Clay Sci.* 29(2): 73-87.
- VILLAR, M.V. 2002. Thermo-hydro-mechanical characterisation of a bentonite from Cabo de Gata. A study applied to the use of bentonite as sealing material in high level radioactive waste repositories. *Publicación Técnica ENRESA 01/2002*. Madrid, 258 pp.
- VILLAR, M.V. & MARTÍN, P.L. 1998. Reseal Project. Annual Progress Report. May 1997-April 1998. Informe Técnico CIEMAT/DIAE/54121/3/98. EC Contract FI4W-CT96-0025. Madrid, 10 pp.
- VILLAR, M.V.; GÓMEZ-ESPINA, R. & GUTIÉRREZ-NEBOT, L. 2012. Basal spacings of compacted bentonite. *Applied Clay Science* 65-66: 95-105.
- VOLCKAERT, G.; DEREEPER, B.; PUT, M.; ORTIZ, L.; GENS, A.; VAUNAT, J.; VILLAR, M.V.; MARTÍN, P.L.; IMBERT, C.; LASSABATÈRE, T.; MOUCHE, E. & CANY, F. 2000. A large-scale in situ demonstration test for repository sealing in an argillaceous host rock. Reseal project – Phase I. EUR 19612. *Commission of the European Communities*, Luxemburg. 273 pp. ISBN 92-894-0095-1.